Journal of Sound and Vibration 329 (2010) 2973–2994

Contents lists available at ScienceDirect

Journal of Sound and Vibration

journal homepage: www.elsevier.com/locate/jsvi

Application of broadband nonlinear targeted energy transfers for seismic mitigation of a shear frame: Computational results

F. Nucera [a], D.M. McFarland [b,*], L.A. Bergman [b], A.F. Vakakis [c,d]

[a] Department of Mechanics and Materials, Mediterranean University of Reggio Calabria, Loc. Feo di Vito, 89122 Reggio Calabria, Italy
[b] Department of Aerospace Engineering, University of Illinois at Urbana-Champaign, 104 South Wright Street, Urbana, IL 61801, United States
[c] Division of Mechanics, School of Applied Mathematical and Physical Sciences, National Technical University of Athens, P.O. Box 64042, GR-157 10 Zografos, Athens, Greece
[d] Department of Mechanical Science and Engineering, University of Illinois at Urbana–Champaign, United States

ARTICLE INFO

Article history:
Received 29 December 2006
Received in revised form
14 November 2009
Accepted 18 January 2010
Handling Editor: M.P. Cartmell
Available online 4 March 2010

ABSTRACT

In this work we show that it is possible to successfully apply the concept of nonlinear targeted energy transfer (TET) to seismic protection of structures; moreover, this passive strategy of seismic vibration control is found to be feasible and robust. We consider a three-story shear-frame structure, modeled as a three-degree-of-freedom system, subjected to four historic earthquakes as seismic excitation. Seismic mitigation is achieved by applying single or multiple nonlinear energy sinks (NESs) to the test structure. We study the performance and efficiency of the NESs through a set of evaluation criteria. First we consider a single vibro-impact NES (VI NES) applied to the top floor of the structure. In order to assess the robustness of the VI NES, the NES parameters are optimized for a specific seismic excitation (Kobe), and then tested against the three other earthquake records to demonstrate effectiveness of the NES for these cases as well. To further improve the effectiveness of the seismic mitigation, we then consider a system of two NESs—an NES with smooth nonlinearity at the top floor of the test structure and a VI NES at the bottom floor. We show that it is indeed possible to drastically reduce the structural seismic response (e.g., displacements, drifts, and accelerations) using this configuration.

1. Introduction

In the context of seismic risk mitigation, it is crucial to be able to diminish as much and as quickly as possible the load induced by vibration and shock energy imparted to a structure by an earthquake. The concept of targeted energy transfer (nonlinear energy pumping) [1,2] appears to be natural for application to seismic mitigation.

In general, the philosophy of structural control design is to confine inelastic deformation primarily to energy dissipaters, while the main structure remains elastic for a design basis earthquake (DBE). At present, no particular damping device (metallic yield, friction, viscoelastic, viscous fluid, tuned mass, or tuned liquid damper) is considered best under all circumstances [3].

In this work we apply a vibro-impact device to the problem of seismic mitigation for the first time. The regular and chaotic dynamics and bifurcations of vibro-impact oscillators have been studied extensively in the literature [4–8]. In an additional series of papers [4,9–15], vibro-impact dampers (VIDs) were considered for reducing the vibration levels of

* Corresponding author. Tel.: +217 649 3853; fax: +217 244 0720.
E-mail address: dmmcf@illinois.edu (D.M. McFarland).

0022-460X/$ - see front matter © 2010 Elsevier Ltd. All rights reserved.
doi:10.1016/j.jsv.2010.01.020

structures under periodic or stochastic excitation. In these it was shown that VIDs can be particularly effective in controlling the vibration of structures, due to significant energy dissipation during inelastic impacts as well as to nonlinear dynamic effects such as momentum transfers during collisions. In the present work we study the dynamics of primary structures with vibro-impact or other nonlinear attachments (and optimize these for seismic mitigation) viewed from a different perspective: that of targeted energy transfer (TET), also known as nonlinear energy pumping [16]. Indeed, instead of viewing the VI attachment as a mere damper, we will examine its capacity to (i) passively absorb and dissipate seismic energy from the primary structure [17,18] and (ii) passively redistribute seismic energy among natural modes of the primary structure, thus enhancing its seismic mitigation properties.

Targeted energy transfer (TET) denotes the one-way (on average), irreversible transfer of energy of vibration from a primary structure to a local attachment with damping and essential stiffness nonlinearity, where the energy is confined and locally dissipated without 'spreading' back to the main structure. The underlying dynamical mechanism causing TET is a p:k transient resonance capture (TRC) [19–21]; that is, an instantaneous internal resonance of the local nonlinear attachment with one of the modes of the main structure, providing the necessary and sufficient conditions for the one-way transfer of energy from the structure to the attachment, which acts as a nonlinear energy sink (NES). As energy decreases due to damping, the conditions for TRC fail, and escape from resonance capture takes place. The merit of applying the energy pumping phenomenon to reduce the seismic response of the primary structure will depend on the ability of the attached NES to passively absorb an adequate portion of the seismic energy on a sufficiently fast time scale that the response of the primary structure is significantly reduced during the crucial initial few cycles of its motion. This was found to be possible and, hence, the proposed nonlinear absorption concept is both feasible and efficacious [17].

The aim of this work is to investigate the potential of using ungrounded NESs (that is, sinks attached only to the primary structure, with no separate connection to ground) for seismic mitigation of a three-story shear frame. The geometric characteristics of the test structure considered herein are those of an experimental structure built in the Linear and Nonlinear Dynamics and Vibrations Laboratory (LNDVL) at the University of Illinois at Urbana–Champaign. First, a vibro-impact nonlinear energy sink (VI NES) is attached to the top floor of the frame (cf. Fig. 1). The reason for attaching the NES to the top floor is that this floor is expected to suffer the highest levels of seismic response and, hence, to excite the VI NES as energetically as possible. It is well known that nonlinear effects in oscillators of the type considered herein are most effective at higher levels of vibrational energy; thus, by attaching the VI NES to the top floor of the frame we attempt to exploit in the most effective way the potentially beneficial effects of the nonlinear attachment for seismic mitigation. We note, however, that a limitation of this attachment location is that the mass of the VI NES must necessarily be restricted to small values compared to the mass of the top floor. On the other hand, the impacts (momentum exchanges) and energy dissipation will be more effective because velocities are higher.

A numerical analysis was carried out utilizing a genetic algorithm to optimize the NES parameters. The criteria that we used to assign quantitative measures to the seismic response of the system were introduced in [22], and are given in terms of maximum and RMS response quantities. The goal of the optimization was to determine the smallest possible value for each criterion [17]. The criteria are stated in a general form, which permits their application to different types of earthquakes. By means of such criteria we can effectively compare the uncontrolled and controlled seismic responses of the 3-dof shear frame. In order to assess the robustness of the VI NES, the NES parameters were optimized for one earthquake and, keeping the NES geometric characteristics fixed, other earthquakes were then considered as base excitation.

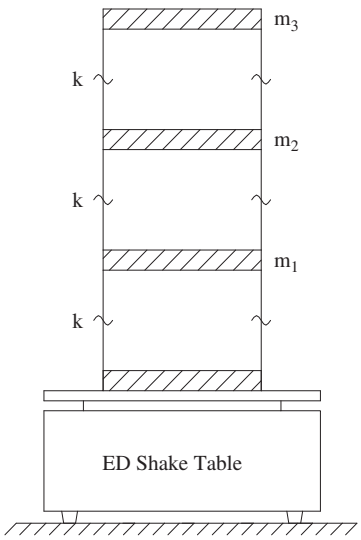

Fig. 1. Schematic of the three-story shear frame.

In addition, through analysis of the relative displacements between the first floor and the ground, the second floor and the first, and the third and the second, we show the occurrence of energy (frequency) scattering towards higher vibration modes [23,24]. This frequency scattering of the seismic energy to structural modes other than those mainly excited by the earthquake in the uncontrolled structure presents a twofold advantage for seismic mitigation. First, it is well established that, for a given input energy, the amplitude of vibration decreases with increasing frequency; due to the vibro-impacts seismic energy is transferred from the low-frequency (but higher-amplitude) first structural mode to the higher-frequency, lower-amplitude structural modes. Also, energy 'leaking' to the lowest structural mode is still beneficial to seismic mitigation, as this mode localizes to the NES. Second, because structural damping dissipation is generally more pronounced in higher structural modes, the high-frequency scattered seismic energy is more effectively dissipated by the structure itself.

To further improve seismic mitigation in the three-story structure, we then considered a two-NES system composed of a VI NES applied to the first floor and an NES with smooth, but essential, cubic stiffness nonlinearity applied to the third floor of the test structure. This two-NES configuration brings two advantages to our seismic mitigation design: (i) for strong near-field earthquakes the VI NES, through its fast reaction time [19,20], can ensure a reduction of the initial peaks of the structural response (immediately after the occurrence of the strong ground motion); (ii) the smooth NES can ensure vibration control of the later structural motion, during the second stage of the response (after the strong ground motion). In addition, the smooth NES is an effective passive vibration boundary controller in cases of earthquakes of modest intensity.

2. Seismic excitations considered

A schematic of the three-story frame considered in this work is depicted in Fig. 1. We study seismic mitigation in this frame by means of passive nonlinear pumping of a significant portion of the applied seismic energy to appropriately designed NESs, where this energy is confined and locally dissipated. To this end, we analyze the dynamics of combined structure-NES models induced by different historical earthquakes. Our purpose is twofold: first, to check the robustness and effectiveness of the NES under different earthquake excitations (testing that the NES design optimal for a specific earthquake produces satisfactory results for other earthquakes); and second, to study NES performance when the energy and frequency content of the earthquake changes (since in nonlinear systems there is in general a strong dependence of the dynamics on input frequency and energy).

Hence, we evaluate our NES-based seismic mitigation concept by considering four distinct historic earthquakes:

(1) El Centro: N–S component recorded at the Imperial Valley Irrigation District substation in El Centro, California, May 18, 1940.
(2) Hachinohe: N–S component recorded at Hachinohe City during the Takochi-oki earthquake of May 16, 1968.
(3) Kobe: N–S component recorded at the Kobe Japanese Meteorological Agency (JMA) station during the Hyogo-ken Nanbu earthquake of January 17, 1995.
(4) Northridge: N–S component recorded at the Sylmar County Hospital parking lot in Sylmar, California, during the Northridge, California earthquake of January 17, 1994.

The ground acceleration records of the four earthquakes are depicted in Fig. 2.

Traditionally, the intensity of a ground motion has, for structural analysis purposes, been defined in terms of peak ground acceleration, which is still widely used as the scaling parameter for ground motion. However, there is increasing evidence that this quantity is a poor measure of the damage potential of an earthquake. Moreover, it is inherently impossible to describe a complex phenomenon, such as the potential of an earthquake to damage civil infrastructure, by a single number, and a great deal of information is inevitably lost when this is attempted. Therefore, three classes of intensity measures (IMs) have been introduced in current seismic mitigation practice.

The first class (Class I) of IMs contains traditional IMs that describe the earthquake source characteristics and time history record. The second (Class II IMs) involves IMs that describe the time history obtained using a single-degree-of-freedom system filter on the original record. Finally, the third class (Class III) of IMs extends this concept to IMs that result from applying an arbitrary filter to the original time history [17,25]. Only Class I and II IMs are considered herein. In Tables 1 and 2 we summarize the IMs of Classes I and II computed for the El Centro, Hachinohe, Kobe and Northridge earthquakes. These tables also show the intensity as reflected in the effective number of cycles N_{cy} [17,26] and the energy content given by the Arias intensity measure I_a. In Table 3 the corresponding effective numbers of cycles are listed. Note that the accelerations are scaled with respect to gravity.

Examining Tables 1 and 2, one can subdivide the aforementioned earthquakes into two groups. The first group, which includes the El Centro and Hachinohe earthquakes, is characterized by relatively long effective ground motion duration T_d and relatively small values of peak ground acceleration (PGA), peak ground velocity (PGV), effective peak acceleration (EPA), and effective peak velocity (EPV). The energy content of the El Centro earthquake is almost twice that of Hachinohe whereas, in terms of CAD and RMS velocity, Hachinohe exhibits greater values (actually, its corresponding CAD is the largest among all the four earthquakes considered herein). In general, all Class I and II intensity measures yield smaller values for the Hachinohe and El Centro earthquakes than for the Kobe and Northridge earthquakes. The largest CAD is

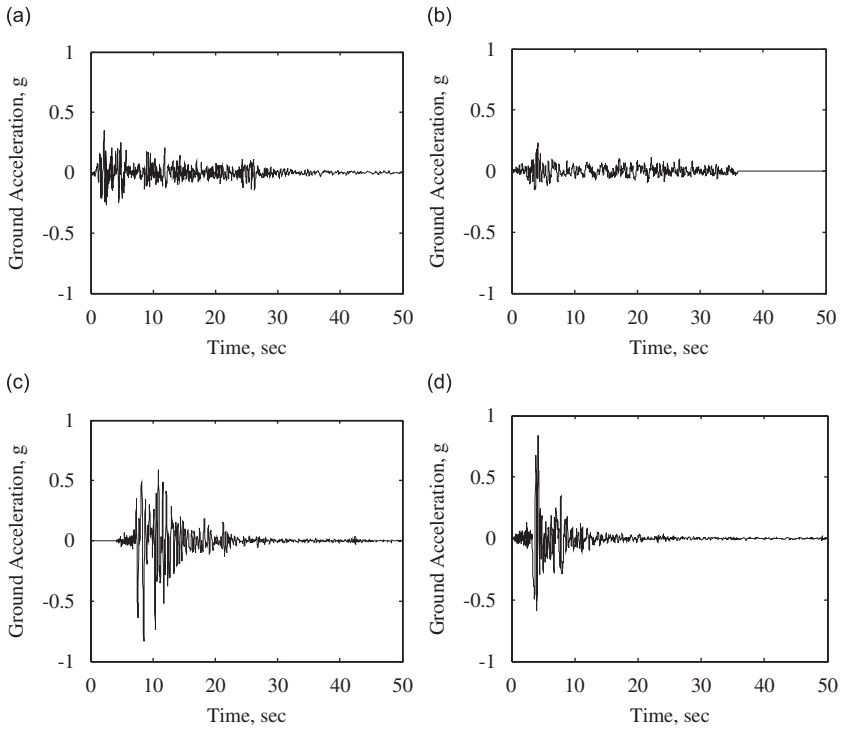

Fig. 2. Ground accelerations of the four historic earthquakes considered in this work.

Table 1
Class I IMs.

Earthquake	IMs						
	T_d (s)	*PGA* (g)	*PGV* (cm/s)	I_a (cm/s)	*CAD* (cm)	V_{rms} (cm/s)	I (cm/s$^{0.75}$)
El Centro	24.41	0.35	34.61	181.93	185.77	8.53	76.94
Hachinohe	27.92	0.23	40.71	90.31	521.33	19.15	93.58
Kobe	8.33	0.83	91.22	838.61	252.99	30.24	154.97
Northridge	5.32	0.84	129.26	500.90	251.40	40.18	196.33

Table 2
Class II IMs.

Earthquake	IMs			
	EPA (g)	*EPV* (cm/s)	*EPD* (cm)	*DSI* (cm)
El Centro	0.28	23.00	9.44	35.43
Hachinohe	0.22	17.39	12.01	45.04
Kobe	0.72	74.74	13.71	51.41
Northridge	0.80	69.56	26.71	100.22

Table 3
Number of effective cycles N_{cy}.

El Centro	Hachinohe	Kobe	Northridge
0.28	0.03	2.13	1.19

associated with the Hachinohe earthquake, but this is merely due to the shape of the signal, depicted in Fig. 2(b); also, the dominant frequency content of the ground velocity for that earthquake is around 0.35 Hz, which is relatively small compared to the other earthquakes. Moreover, this earthquake has the lowest EPA (one of the more suitable parameters for

choosing a test earthquake, together with EPV), which supports the observation that Hachinohe exhibits the smallest energy content (I_a) and, thus, the lowest destructive capacity. El Centro should be viewed as a medium-intensity earthquake (compared, for instance, with the Northridge earthquake), with energy approximately 35% of that of Northridge; similar comparisons hold for all Class II IMs.

In the second group we include the earthquakes of Kobe and Northridge. These are characterized by relatively short effective ground motion duration and large values of PGA, PGV, EPA, and EPV. Comparing the Kobe earthquake to the Northridge, Kobe has the higher energy content (I_a is 67% larger), approximately the same PGA, and 10% smaller EPA, but 6% greater EPV.

That the Kobe earthquake exhibits the largest effective number of cycles (above the low-amplitude cut-off) confirms that it is the one with the greatest destructive capacity (almost twice that of Northridge) (cf. Table 3). With $N_{cy}=2.13$, and taking into account that only the zero-crossing peaks are considered, the Kobe could be viewed as an earthquake which exhibits two complete cycles with 1 g amplitude. In other words, the Kobe earthquake can be decomposed into two complete cycles of sine waves each having amplitude 1 g. This gives a clearer picture of how much energy is carried, and how it is applied to the structure over time. Also, the largest value of the energy IM, I_a, is associated with the Kobe earthquake, which supports our selection of it as the main test earthquake in the study.

3. Single VI NES connected to the top floor of the three-story frame (NES Design I)

The first NES design considered in this work consists of a single VI NES attached to the top floor of the test structure, as depicted in Fig. 3(a). In the following discussion, the frame will also be referred to as the primary system. The geometric and material properties of the test structure are those of an experimental fixture available for later testing. For the numerical simulations reported here, we model the three-story structure as a three-degree-of-freedom system, as shown in Fig. 3(b), with equal masses $m_1=m_2=m_3=1.127$ kg and interstory stiffnesses $k=5000$ N/m.

The modal damping ratios assumed for the model are identical to those identified through experimental modal analysis of the experimental fixture. The modal analysis has been carried out through two different techniques. The first, Ibrahim time domain (ITD), works in the time domain and uses the free-response time histories from the structure under test; the second, rational fraction polynomial (RFP) curve fit, works in the frequency domain and estimates the modal parameters by curve-fitting the experimental frequency response functions. The ITD analysis was done in Matlab® whereas the RFD was performed using Diamond®. The results of the modal identification through the aforementioned techniques are summarized in Table 4, where we report the modal damping ratios together with the mode shapes found with each identification technique. Hence, for the numerical simulations in this work we assume the following viscous damping ratios for the three modes of the model: $\zeta_1=0.275\%$, $\zeta_2=0.313\%$, and $\zeta_3=0.236\%$. The other structural modal parameters identified through modal analysis of the experimental frame are natural frequencies, $f_1=4.6$, $f_2=12.8$, and $f_3=18.3$ Hz; effective modal masses, $\gamma_1=3.317$, $\gamma_2=0.266$, and $\gamma_3=0.038$ kg; and modal participation factors, $\Gamma_1=1.23$, $\Gamma_2=0.34$, and $\Gamma_3=-0.13$.

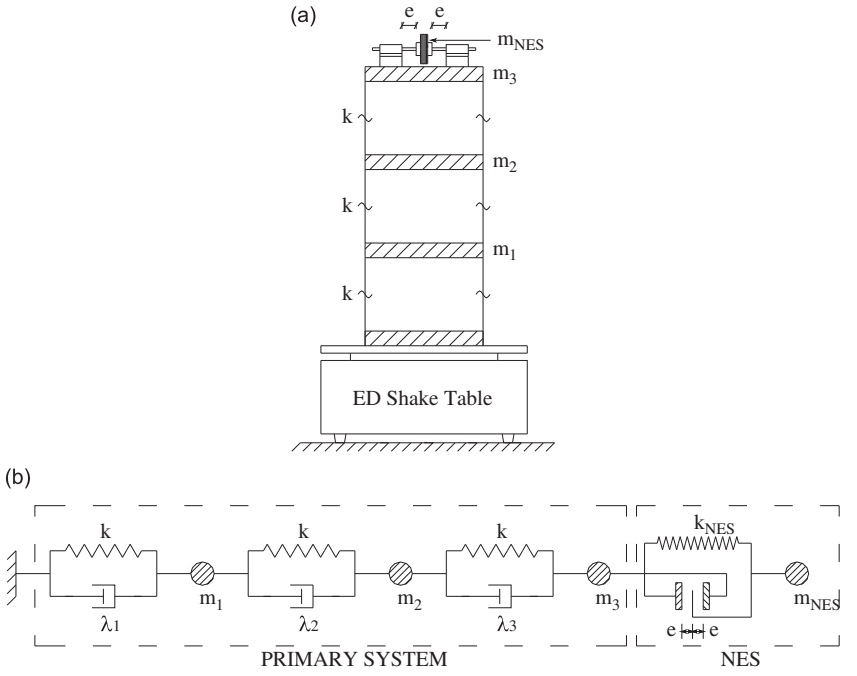

Fig. 3. NES Design I: Three-story shear frame with VI NES at the top floor: (a) schematic and (b) model.

Table 4
Measured mode shapes and estimated modal damping ratios.

ITD					RFP				
Mode	Dof			Damping ratio (%)	Mode	Dof			Damping ratio (%)
	1	2	3			1	2	3	
1	0.32	0.87	1.00	0.291	1	0.35	0.91	1.00	0.257
2	1.00	0.32	−.94	0.311	2	1.00	0.32	−.90	0.314
3	−.65	1.00	−.58	0.230	3	−.65	1.00	−.56	0.242

The model of the primary system (the three-story shear frame) is governed by the linear equation of motion

$$M\ddot{u}+C\dot{u}+Ku=-M\Gamma\ddot{u}_g, \tag{1}$$

where the mass and stiffness matrices and the relative displacement vector (with respect to ground) are

$$M=\begin{bmatrix} m_1 & 0 & 0 \\ 0 & m_2 & 0 \\ 0 & 0 & m_3 \end{bmatrix}, \quad K=\begin{bmatrix} 2k & -k & 0 \\ -k & 2k & -k \\ 0 & -k & k \end{bmatrix}, \quad u(t)=\begin{Bmatrix} u_1(t) \\ u_2(t) \\ u_3(t) \end{Bmatrix}, \tag{2}$$

$\ddot{u}_g$ represents the ground acceleration, and Γ is the pseudo-static vector.

We consider the case where the primary system is proportionally viscously damped. With the modal damping ratios referenced above we compute the damping matrix from

$$\hat{C}=\Phi^T C\Phi, \tag{3}$$

where Φ is the modal matrix normalized with respect to M, $\hat{C}$ is defined as

$$\hat{C}=\begin{bmatrix} 2\zeta_1\omega_1 & 0 & 0 \\ 0 & 2\zeta_2\omega_2 & 0 \\ 0 & 0 & 2\zeta_3\omega_3 \end{bmatrix}, \tag{4}$$

and ω_j, j=1, 2, 3, is the j-th natural frequency of the primary system in rad/s.

A strongly nonlinear, vibro-impact NES (VI NES) was attached to the top (third) floor of the shear frame as shown in Fig. 3. The mass and stiffness matrices of the combined system become

$$M=\begin{bmatrix} m_1 & 0 & 0 & 0 \\ 0 & m_2 & 0 & 0 \\ 0 & 0 & m_3 & 0 \\ 0 & 0 & 0 & m_{\mathrm{NES}} \end{bmatrix}, \quad K=\begin{bmatrix} 2k & -k & 0 & 0 \\ -k & 2k & -k & 0 \\ 0 & -k & k+k_{\mathrm{NES}} & -k_{\mathrm{NES}} \\ 0 & 0 & -k_{\mathrm{NES}} & k_{\mathrm{NES}} \end{bmatrix}, \tag{5}$$

while in the damping matrix a zero row and column are added at the NES degree of freedom.

The system composed of the primary structure with the attached VI NES is piece-wise linear. This is because during the time interval that separates two consecutive impacts the system is purely linear. Hence, the numerical integration of the equations of motion (EOM) of the combined system is performed by solving a sequence of linear initial value problems (IVPs), each of which is bounded by two consecutive vibro-impacts of the NES. In this context, the computation of the precise time instants when the vibro-impacts occur is crucial for the accurate simulation of the overall transient nonlinear dynamics, since these time instants determine the boundaries of the numerical integrations of the sequence of linear problems. When an impact occurs, the computation is stopped, the initial conditions are appropriately modified to account for the state of the system after the impact, and the numerical integration resumes. The relation linking the velocities of the colliding masses of the VI NES before and after each impact is given by the well known expression

$$v_3'-v_{\mathrm{NES}}'=r(v_3-v_{\mathrm{NES}}), \tag{6}$$

where v'_3 is the velocity of the mass m_3 after the impact, v'_{NES} is the velocity of the NES mass after the impact, r is the coefficient of restitution, v_3 is the velocity of the mass m_3 before the impact, and v_{NES} is the velocity of the NES mass before the impact. The energy that both masses m_3 and m_{NES} exhibit before the impact is not conserved during the impact because r is less than unity, but the momentum is preserved; thus, it holds that

$$m_3v_3+m_{\mathrm{NES}}v_{\mathrm{NES}}=m_3v_3'+m_{\mathrm{NES}}v_{\mathrm{NES}}'. \tag{7}$$

Using a numerical method with a fixed time step, the solution of the equations of motion may well be problematic, depending on the size of the step. For this reason, and to ensure that the activation of the non-smooth nonlinearity is correctly modelled during the transient motion, the solution of the system is sought in phase space using the Matlab

function ode45, which utilizes an adaptive time step. The equations of motion in phase space are expressed as

$$\dot{y} = Ay + F, \tag{8}$$

where y and $\dot{y}$ are the state vector and its time derivative, respectively, given by

$$y = \begin{bmatrix} u \\ \dot{u} \end{bmatrix}, \quad \dot{y} = \begin{bmatrix} \dot{u} \\ \ddot{u} \end{bmatrix}, \tag{9}$$

and the system matrix A and the input matrix F are expressed

$$A = \begin{bmatrix} 0 & I \\ -M^{-1}K & -M^{-1}C \end{bmatrix}, \quad F = \begin{bmatrix} 0 \\ -\Gamma \ddot{u}_g \end{bmatrix}. \tag{10}$$

The differential Eqs. (8) are integrated by using the Runge-Kutta method with non-uniform time step. Accurate determination of the time instant of each impact is achieved by imposing a sufficiently small tolerance (e.g., 10^{-8}). In the numerical algorithm, the condition of impact is represented by

$$e - \text{tol} \le |u_r| \le e + \text{tol}, \tag{11}$$

where e is the clearance of the VI NES (cf. Fig. 3(b)); tol, the tolerance; and $u_r = u_{\text{NES}} - u_3$, the relative displacement between the NES mass and the rigid constraints.

We mention at this point that this class of problems is especially challenging from the analytical and computational points of view, since the time instants when the vibro-impacts occur are determined by the solution itself and not a priori. Moreover, the essential (strong) nonlinearity of the system is generated precisely at these time instants (due to the impulsive excitations applied to the integrated system); and in addition, at exactly these time instants, significant portions of energy are dissipated due to inelastic collisions between the NES mass and mass m_3. It follows that in order to computationally model this class of problems correctly one must pay special attention to the accurate computation of the time instants where the vibro-impacts occur, as well as the energy dissipated during each impact [27].

3.1. Optimization study for Northridge excitation

The VI NES parameters (mass m_{NES}, stiffness k_{NES}, clearance e, and coefficient of restitution r) were optimized through the use of a set of evaluation criteria. The criteria utilized to assign quantitative measures to the seismic response of the system were introduced in [22]. The goal of the optimization was to determine the smallest possible output value for each criterion (with the exception of the last indicator, where the maximum was sought).

The technique employed to optimize the parameters of the NES is a global method called differential evolution [28,29]. This method belongs to the class of evolutionary computations. Each computed evaluation criterion represents, by definition, the maximum value among the maxima of a certain quantity computed with respect to the four different earthquakes (cf. Table 5). In this particular case, each criterion was computed over time for each of the earthquakes separately with the purpose of optimizing the NES parameters for that specific earthquake; the goal was to minimize an objective function defined as $OF = J_1 + J_2 + J_5 + J_6$, where the evaluation criteria are given in Table 5.

Table 5
Definitions of the evaluation criteria.

Evaluation criterion	Related structural response variable	Expression*
J_1	Maximum absolute floor displacement (with respect to ground)	$J_1 = \max_{\text{earthquakes}} \{\max_{\substack{t \\ i\in\eta}} \lvert u_i(t)\rvert / u^{max}\}$
J_2	Maximum interstory drift	$J_2 = \max_{\text{earthquakes}} \left\{ \frac{\max_{t,i} (\lvert d_i(t)\rvert / h_i)}{d_n^{max}} \right\}$
J_3	Maximum absolute floor acceleration (with respect to ground)	$J_3 = \max_{\text{earthquakes}} \{\max_{\substack{t \\ i\in\eta}} \lvert \ddot{u}_{ai}(t)\rvert / \ddot{u}_a^{max}\}$
J_4	Maximum inertial force at each dof	$J_4 = \max_{\text{earthquakes}} \{\max_{t} \lvert \sum_{i\in\eta} m_i \ddot{u}_{ai}(t)\rvert / F_b^{max}\}$
J_5	Maximum normed floor displacement with respect to the ground	$J_5 = \max_{\text{earthquakes}} \{\max_{i\in\eta} \lVert u_i(t)\rVert / \lVert u^{max}\rVert\}$
J_6	Maximum normed interstory drift	$J_6 = \max_{\text{earthquakes}} \{\max_{t,i} (\lVert d_i(t)\rVert / h_i) / \lVert d_n^{max}\rVert\}$
J_7	Maximum normed absolute floor acceleration (with respect to ground)	$J_7 = \max_{\text{earthquakes}} \{\max_{i\in\eta} \lVert \ddot{u}_{ai}(t)\rVert / \lVert \ddot{u}_a^{max}\rVert\}$
J_8	Maximum normed inertial force at each dof	$J_8 = \max_{\text{earthquakes}} \left\{ \frac{\lVert \sum_{i\in\eta} m_i \ddot{u}_{ai}(t)\rVert}{\lVert F_b^{max}\rVert} \right\}$

* For all criteria the quantities at denominator refer to numerators are computed for the controlled structure.

The historic Northridge earthquake was the base excitation considered for the first optimization study of the NES. In order to place the frequency content of the earthquake closer to the structural frequency spectrum (and, thus, study the seismic response under the most severe possible conditions), we scaled the historic earthquake by compressing its original duration from 50 to 25 s, thus increasing its characteristic frequencies by a factor of two.

We observed that during the strong ground motion the VI NES acts very quickly and there are several vibro-impacts that dissipate a significant amount of energy (this is the reason why evaluation criteria J_3 and J_4, as well as J_7 and J_8, are not included in the objective function). This is one advantage of applying a strongly nonlinear energy sink (i.e., the VI NES) rather than a smooth NES (which exhibits a slower reaction time) for mitigation of the higher peaks of the structural seismic response. In a later alternative design, a smooth NES is applied to the problem of seismic mitigation in conjunction with a VI NES [17,18]. It has been demonstrated that the smooth nonlinear sink possesses the important characteristic of broadband shock energy absorption and dissipation as, depending on its instantaneous energy and due to its essentially nonlinear (nonlinearizable) stiffness, the NES can resonate with structural modes of the primary system lying in arbitrary frequency ranges [1,30–33].

The optimized VI NES parameters for the Northridge earthquake were determined to be m_{NES}=4% (of the total mass of the primary system), k_{NES}=0.005*k (linear stiffness), r=0.4 (coefficient of restitution), and e=0.02 m (clearance). The natural frequencies of the linear integrated system (i.e., the system obtained by considering the primary system connected through the weak linear spring k_{NES} to the NES mass) are f_1=2.2, f_2=4.6, f_3=12.8, and f_4=18.3 Hz. We conclude that the addition of a weakly coupled, lightweight attachment to the top floor introduces a new (lowest) natural frequency at 2.2 Hz.

In Fig. 4, the comparison between the controlled and uncontrolled displacements (with respect to ground) for each floor of the frame and the optimized NES displacement are depicted. Fig. 5(a) shows the absolute displacements of the third floor of the primary system and the optimized VI NES; Fig. 5(b), the phase plot of the relative displacement between the third floor and the NES versus its time derivative (relative velocity); and Fig. 5(c), the portion of instantaneous total energy dissipated during each vibro-impact as well as the time history of vibro-impacts at the NES. This last plot helps to identify the severity of vibro-impacts and, thus, determine if the VI NES interacts sufficiently with the primary system. A high value of this fraction indicates an efficient vibro-impact, as a larger amount of the total instantaneous energy of the structure is dissipated during the vibro-impact considered.

The wavelet spectra of the relative displacements between the first floor and the ground, the second floor and the first, and the third floor and the second are depicted in Fig. 6. The wavelet transform (WT) can be considered as a 'dynamic' extension of the 'static' Fourier transform (FT), in the sense that instead of decomposing a time series (signal) in the frequency domain using cosine and sine trigonometric functions (as in the FT), alternative families of orthogonal functions are employed which are localized in frequency and time. These families of orthogonal functions, the so-called wavelets, can be adapted in time and frequency to provide details of the frequency components of the signal during the time interval that is analyzed. These wavelets result from a mother wavelet function through successive iterations. As a result, the WT provides the transient evolution of the main frequency components of the time series. In this work the numerical WT was

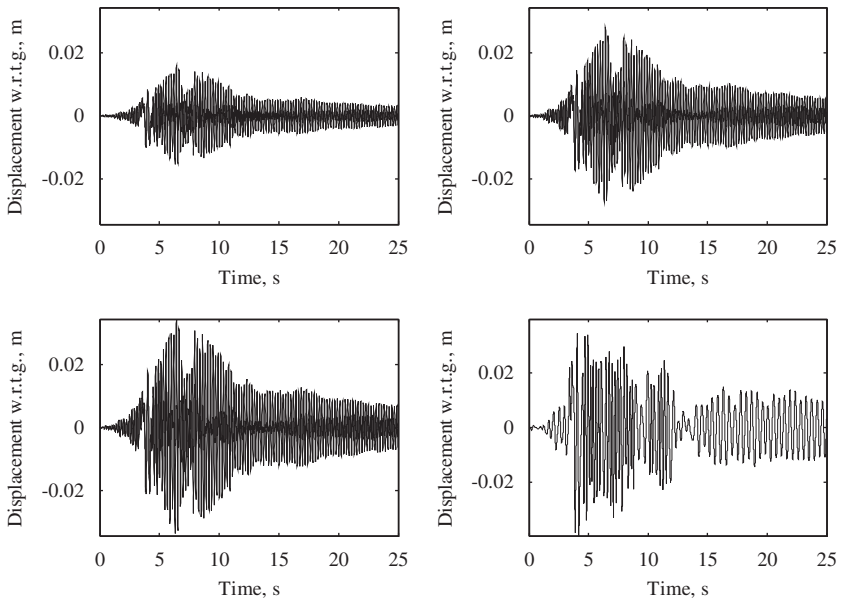

Fig. 4. Uncontrolled and controlled displacements when an optimized VI NES is attached to the third floor of the frame, for Northridge seismic excitation; u_j is the absolute displacement of the j-th floor. Dashed line, without NES; solid line, with NES.

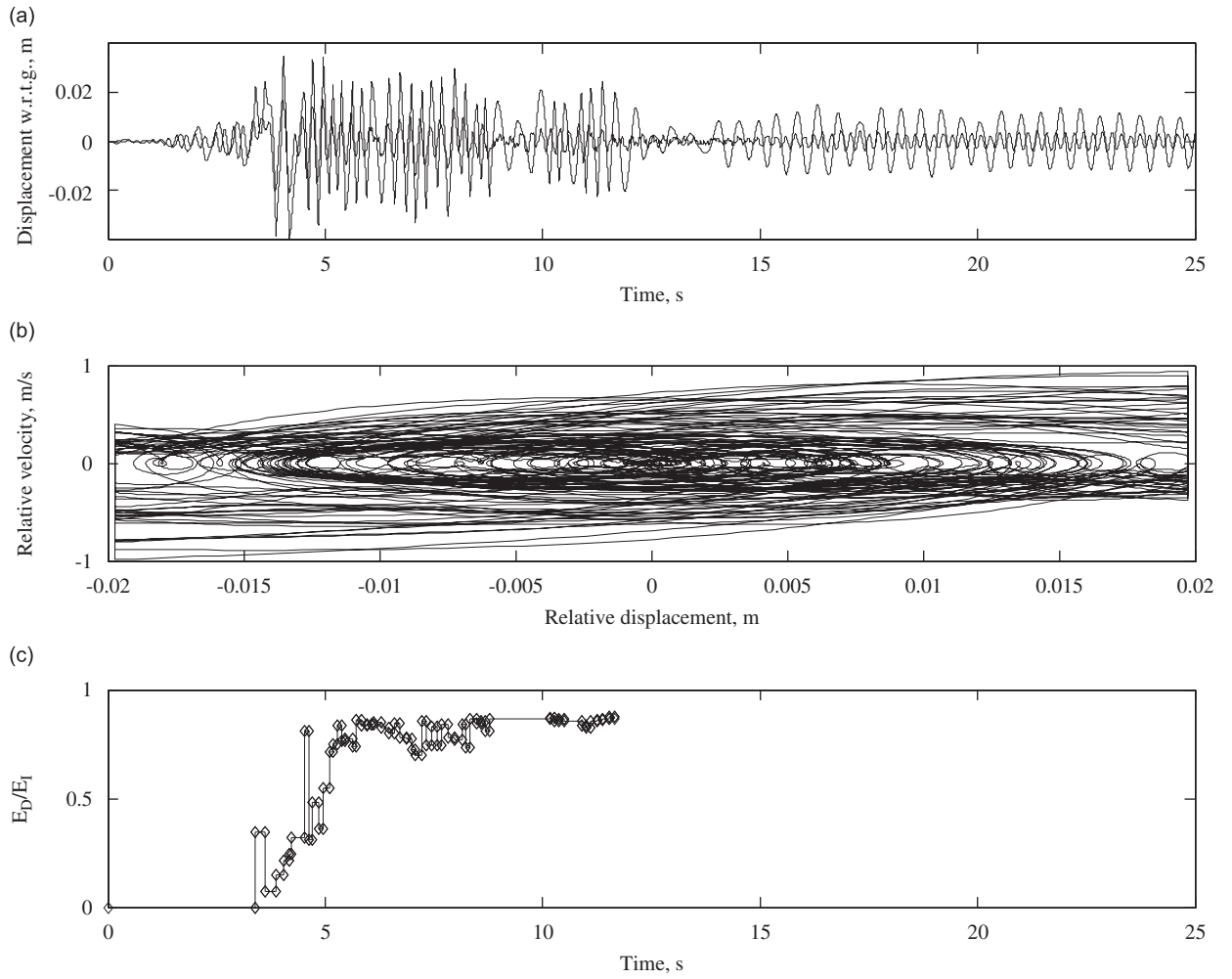

Fig. 5. Performance of the optimized VI NES for Northridge seismic excitation: (a) comparison between absolute displacements of the third floor (darker line) and the NES (lighter line); (b) phase plot of relative displacement between the third floor and the NES; and (c) energy transaction by the VI NES (portion of instantaneous seismic energy dissipated during each vibro-impact).

performed using a Matlab code developed at Université de Liège. The code employs the Morlet mother wavelet, a Gaussian-windowed complex sinusoid of frequency ω_0 rad/s, $\psi_M(t) = e^{-t^2/2}e^{j\omega_0 t}$. The frequency ω_0 is the user parameter which enables one to tune the frequency and time resolution of the results [5,24].

From the wavelet spectra of Fig. 6, we clearly observe the frequency scattering of seismic energy to all structural modes due to the vibro-impacts at the NES. Indeed, examining the uncontrolled relative displacements, we see that the seismic response is mainly confined to the first structural mode (close to 4.6 Hz), which explains the relatively high seismic response of the uncontrolled frame. This is common in unprotected structures which, under seismic excitation, typically respond in their lowest mode and, in essence, behave approximately as single-dof oscillators. On the contrary, considering the controlled relative displacements, the seismic energy is scattered to as many as four modes, ranging from the lowest at 2.2 Hz (which results due to the weak linear coupling spring of the NES and is localized to the NES) to the highest mode at 18.3 Hz; moreover, the frequency scattering becomes stronger and more evident at the higher floors. This frequency scattering of the seismic energy to modes other than the leading structural mode at 4.6 Hz presents a twofold advantage for seismic mitigation, and explains the drastically reduced structural response depicted in Fig. 4. First, it is well established that the level of vibration is smaller at higher-frequency structural modes; hence, due to the vibro-impacts, seismic energy is transferred from the low-frequency (but high-amplitude) first structural mode to the lower-amplitude, higher-frequency structural modes. In addition, energy 'leaking' to the lowest structural mode, at 2.2 Hz, results in even more seismic mitigation, as this mode localizes to the NES. Second, since structural damping dissipation is more effective at higher structural modes, high-frequency seismic energy is more effectively dissipated by the structure itself. As a result, the overall vibration levels of the controlled frame are dramatically reduced.

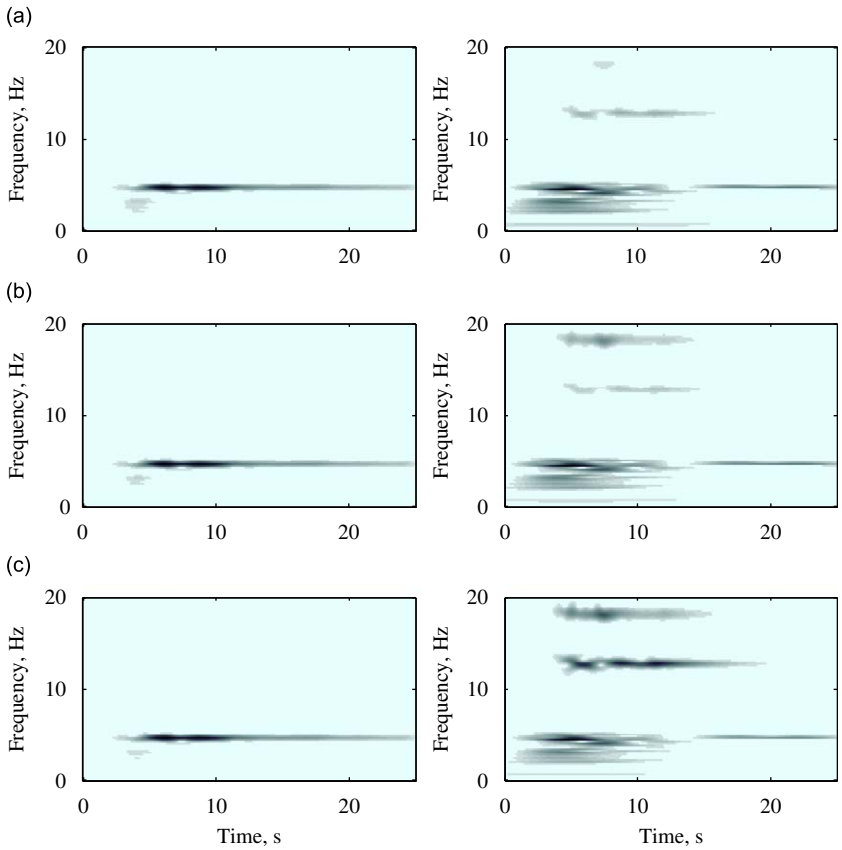

Fig. 6. Comparisons between the wavelet spectra of uncontrolled (left column) and controlled (right column) relative displacements for a primary system with optimized VI NES attached to the third floor, and Northridge seismic excitation: (a) $u_1(t)-u_g(t)$, (b) $u_2(t)-u_1(t)$, $u_2(t)-u_1(t)$, and (c) $u_3(t)-u_2(t)$.

In this case the performance of the optimized NES can be evaluated through the eight criteria defined previously, yielding

J_1	J_2	J_3	J_4	J_5	J_6	J_7	J_8
0.61	0.59	0.80	0.58	0.37	0.39	0.57	0.39

We observe a 39% reduction in maximum displacement and a 41% reduction in maximum interstory drift. Moreover, the reduction in the normed evaluation criteria are also quite significant.

Considering the controlled seismic responses in more detail, it is possible to recognize the following three different phases of the response. During the first three seconds, the relative motion between the NES and the third floor of the frame is smaller than the clearance so that no vibro-impacts occur (cf. Fig. 5(c)); hence, the response of the system is linear in this initial phase of the response.

The second phase of the response is characterized by the occurrence of 1:1 resonance capture [19,34,35] between the first structural mode and the VI NES, during which efficient targeted energy transfer of seismic energy from the primary system to the VI NES (and local dissipation there) occurs through a vigorous series of vibro-impacts, and strong dissipation of seismic energy takes place (cf. Fig. 5(c)). This resonance capture regime holds for about 5.5 s (from 3 to 8.5 s), during which a large amount of seismic energy is dissipated (about 87%); this is consistent with earlier results [30,31,35] where it was found that resonance captures between modes of the primary structure and an attached NES are very efficient mechanisms for targeted transfers of shock energy.

After escape from resonance capture the third phase of the response takes place, where a series of vibro-impacts occurs (approximately between 10 and 12 s), during which seismic energy dissipation is not as effective (cf. Fig. 5(c)). It must be noted, however, that after the initial 8 s the earthquake has already released nearly all its energy. Thus, the energy remaining to dissipate in the system is small and motion is mainly localized to the NES. Therefore, if we consider that the energy ratio is computed with respect to the total energy in the integrated assembly (which includes the NES), we can state that the energy dissipated in an extremely short time (during the aforementioned second phase of the motion) is of the order of 90%. A desirable side-effect of this is that the structure itself does not experience large oscillations during the

period of strong ground motion. This confirms that the VI NES is effective from the very beginning of the structural response and is able to dissipate seismic energy on a sufficiently fast time scale. Thus, the VI NES exhibits a suitably short 'reaction time' and dissipates a major portion of seismic energy through efficacious vibro-impacts. This provides the first mechanism for seismic energy dissipation in this vibro-impact design.

The second mechanism, also triggered by vibro-impacts, is the aforementioned frequency scattering of seismic energy to all structural modes (even though these modes are not directly excited by the earthquake in the uncontrolled primary structure). Examination of Fig. 6 reveals clearly that the system with attached VI NES initially vibrates predominantly in its fundamental mode; this is to be expected as, in the initial phase of the response, no vibro-impacts occur and the response is linear. After approximately 4 s (i.e., when the resonance capture regime of the response begins) the other three structural modes of the integrated system are excited by the repeated vibro-impacts at the NES. The higher-frequency structural modes exhibit greater dissipation and smaller modal amplitudes, whereas the lowest mode localizes at the NES. Hence, effective dissipation of seismic energy takes place.

Moreover, as first shown in [16] and confirmed in this work, due to the extremely short reaction time of the VI NES (or equivalently, the fast scale of the VI dynamics), the conditions for 1:1 TRC between the VI NES and the structure are realized in the critical initial stage of the motion where the seismic energy of the primary system is at its highest. Hence, the fast time scale of TET in the vibro-impact case enables the VI NES to passively absorb a large portion of the seismic energy from the primary structure during the high-energy initial regime of the motion (during the critical first cycles of seismic response), and to efficiently dissipate it through inelastic impacts—which have been proven to be a very efficient mechanism for damping dissipation [27]. This results in a significant reduction of the maximum levels of seismic response of the primary structure, which is essential for effective seismic protection. Because such fast-scale TET cannot be realized with NESs with smooth (continuous) stiffness nonlinearities, one concludes that the discontinuous nature of the VI NES is key to the success of the TET-based seismic mitigation design proposed in this work.

3.2. Optimization study for Kobe excitation

To further investigate the performance and the efficacy of NES Design I, we also optimized the VI NES for the Kobe seismic excitation. This additional optimization study tested the robustness of the proposed design to changes in seismic input. As in the case of the Northridge earthquake, in order to 'tune' the earthquake frequency content to the range of the natural frequencies of the linear structure (and to make the seismic excitation as severe as possible), the historic Kobe earthquake record was time-scaled to 25 s from its original duration of 50 s.

An ungrounded VI NES was applied to the third floor of the primary structure; then, through the genetic algorithm described in Section 3.1, the following optimal NES parameters were computed: m_{NES}=4.5% (of the total mass),

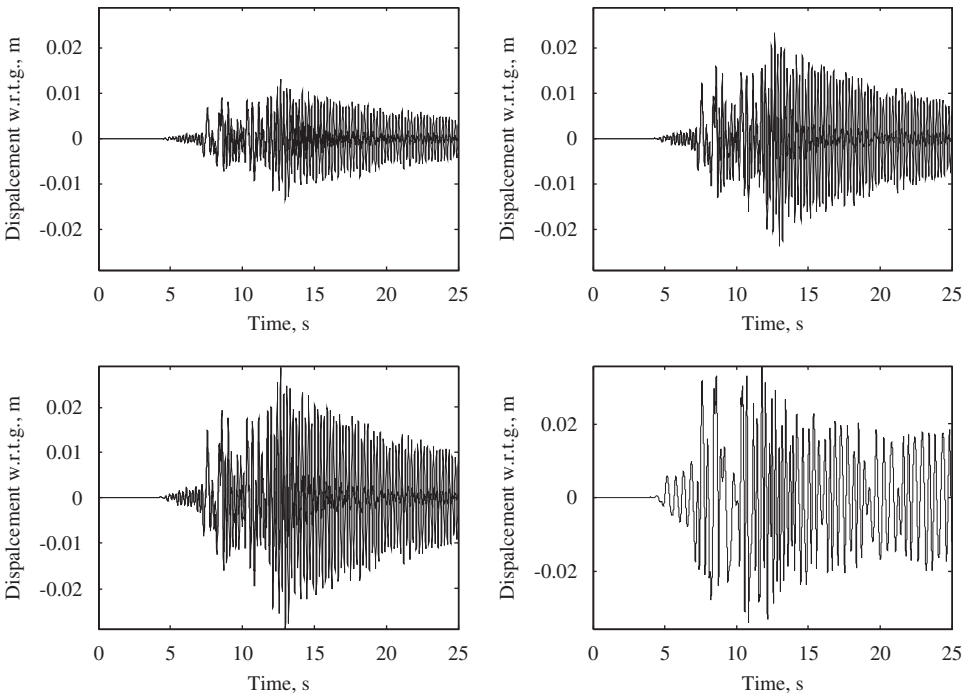

Fig. 7. Uncontrolled and controlled displacements when an optimized VI NES is attached to the third floor of the frame, for Kobe seismic excitation; u_j is the absolute displacement of the j-th floor. Dashed line, without NES; solid line, with NES.

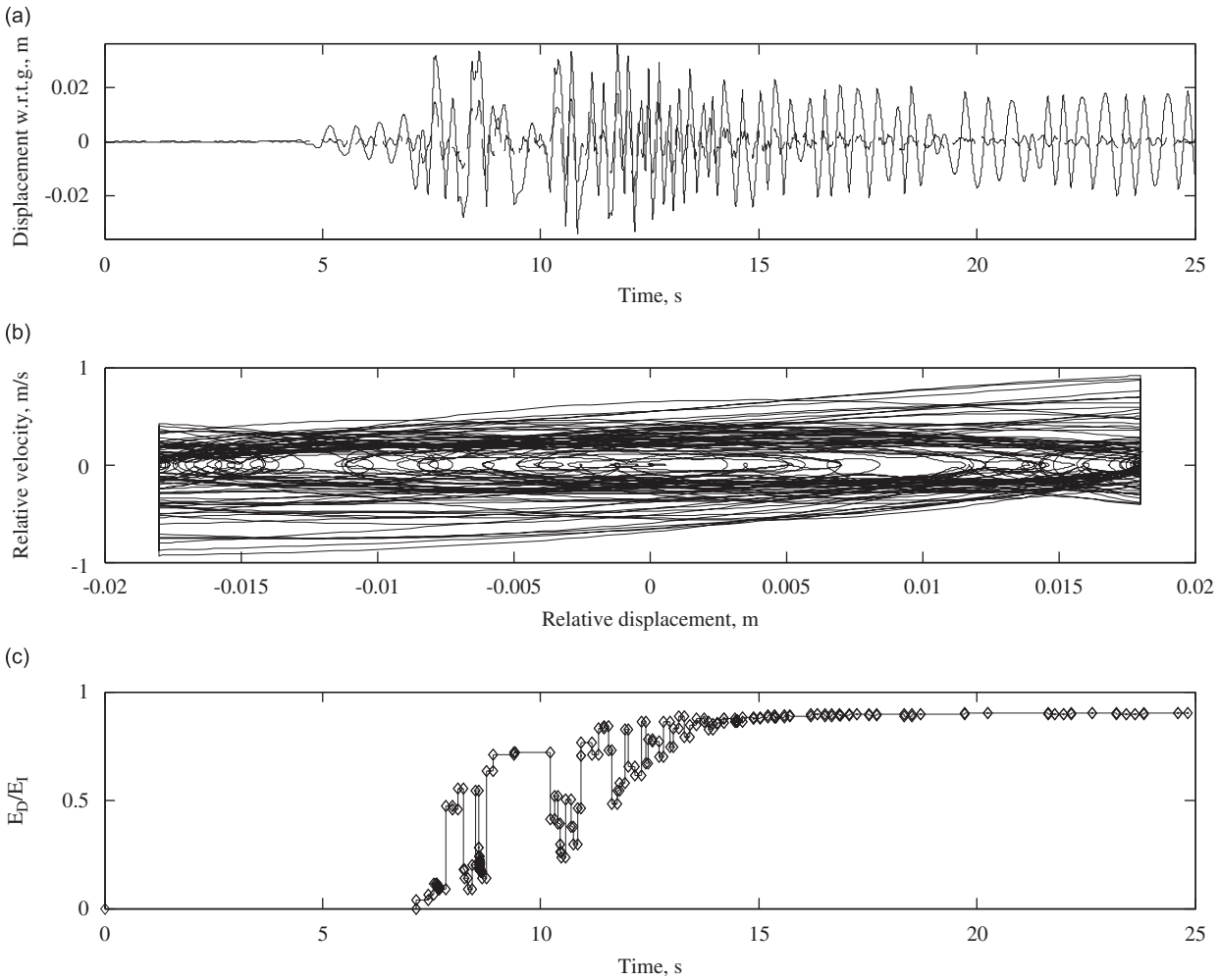

Fig. 8. Performance of the optimized VI NES for Kobe seismic excitation: (a) comparison between absolute displacements of the third floor (darker line) and the NES (lighter line); (b) phase plot of relative displacement between the third floor and the NES; and (c) energy transaction by the VI NES (portion of instantaneous seismic energy dissipated during each vibro-impact).

$k_{NES}=0.004^{*}k$ (linear stiffness), $r=0.4$ (coefficient of restitution), and $e=0.018$ m (clearance). The resulting natural frequencies of the linearized system (with NES attached but with no impact, i.e., with large clearance) are $f_1=1.7$, $f_2=4.6$, $f_3=12.8$, and $f_4=18.3$ Hz.

In Fig. 7 we present the comparison between the controlled and uncontrolled relative displacements (as defined earlier) for each floor of the system, together with the relative NES displacement with reference to the ground. Fig. 8 depicts the displacements of the third floor and the VI NES together with a plot of the projection of the phase space consisting of relative velocity versus relative displacement between the third floor and the NES; also presented in Fig. 8 is a plot of the amount of energy dissipated during each vibro-impact as a portion of the total instantaneous energy of the system when this impact occurs. These plots indicate that there occurs a series of very efficient vibro-impacts that dissipate a significant portion of the seismic energy at the early (high-energy) stage of the motion.

Following the practice introduced in the previous section, in Fig. 9 the wavelet transforms (WTs) of the relative displacements of the uncontrolled and controlled structure are depicted. These plots clearly prove that when the uncontrolled linear structure is excited by the Kobe earthquake its response involves predominantly the first structural mode (hence, the relatively large structural responses). The addition of the VI NES scatters the seismic energy to a relatively wide band of frequencies, ranging from the lowest mode, close to 1.7 Hz (which appears due to the weak linear stiffness of the NES and is localized to the NES), to the highest structural mode at 18.3 Hz; the beneficial effects to seismic mitigation of this seismic energy scattering were discussed in detail in the previous section. We again conclude that the VI NES is not only capable of efficiently dissipating the seismic energy through inelastic vibro-impacts, but also proves to be an efficient scatterer of seismic energy to structural modes other than the one that is directly excited by the earthquake in the uncontrolled structure.

In order to assess the robustness of the VI NES as a mitigation device, the design optimized for the Kobe earthquake was subjected to the other historic earthquakes introduced in Section 2. The aim of this exercise was to determine if a single

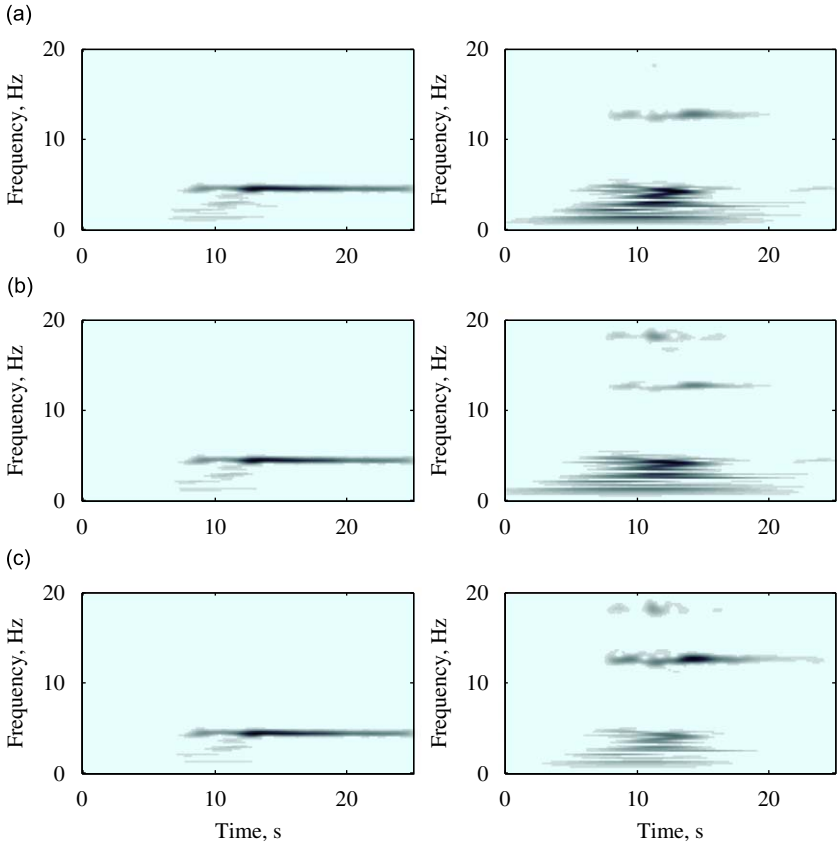

Fig. 9. Comparisons between the wavelet spectra of uncontrolled (left column) and controlled (right column) relative displacements for a primary system with optimized VI NES attached to the third floor, and Kobe seismic excitation: (a) $u_1(t)-u_g(t)$, (b) $u_2(t)-u_1(t)$, and (c) $u_3(t)-u_2(t)$.

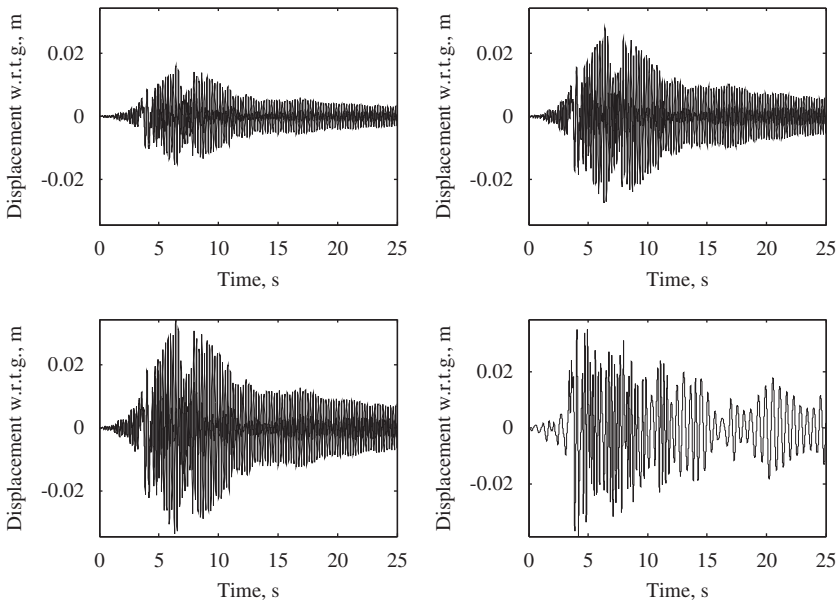

Fig. 10. Uncontrolled and controlled displacements when an optimized VI NES (based on Kobe seismic excitation) is attached to the third floor of the frame, for Northridge seismic excitation; u_j is the absolute displacement of the j-th floor. Dashed line, without NES; solid line, with NES.

NES design is capable of drastically reducing the seismic response of the frame subject to each of the four earthquakes. In Figs. 10–12 comparisons between the controlled and uncontrolled displacements for the three floors of the frame as well as the absolute NES displacement, all referenced to ground, are presented for each of the aforementioned

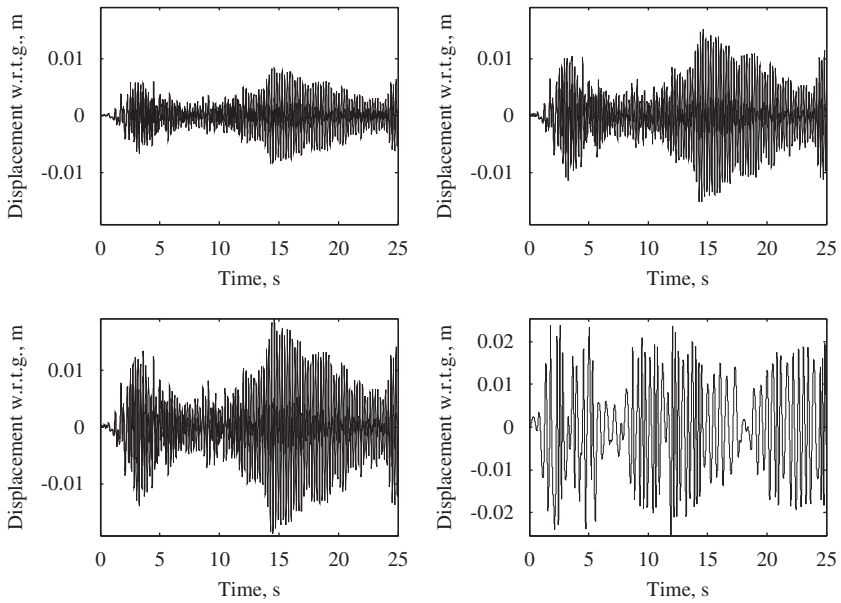

Fig. 11. Uncontrolled and controlled displacements when an optimized VI NES (based on Kobe seismic excitation) is attached to the third floor of the frame, for El Centro seismic excitation; u_j is the absolute displacement of the j-th floor. Dashed line, without NES; solid line, with NES.

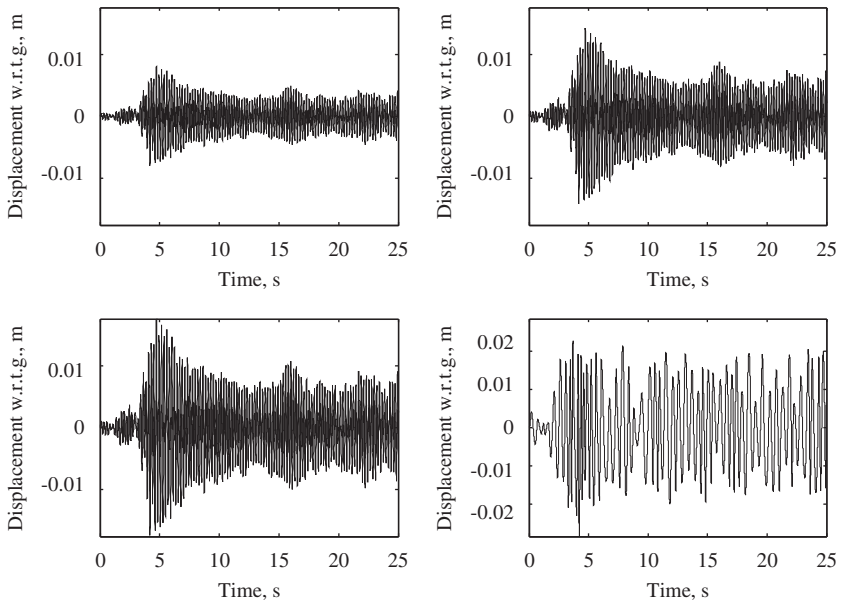

Fig. 12. Uncontrolled and controlled displacements when an optimized VI NES (based on Kobe seismic excitation) is attached to the third floor of the frame, for Hachinohe seismic excitation; u_j is the absolute displacement of the j-th floor. Dashed line, without NES; solid line, with NES.

earthquakes. From these results we conclude that dramatic reduction of the seismic response was achieved in every case.

The performance of the optimized VI NES based on the Kobe seismic excitation, when the primary structure is excited by each of the four test earthquakes, was measured via the eight evaluation criteria introduced earlier; the numerical results are summarized in Table 6. For the Kobe earthquake, reductions of 36% for the maximum displacement (J_1) and 38% for the maximum interstory drift (J_2) were observed, and again the normed evaluation criteria were significantly reduced (to 42% and 45% for J_5 and J_6, respectively). In the Northridge case, a reduction of 36% for both maximum displacement and

Table 6
Summary of the evaluation criteria for different earthquakes, VI NES at the top floor.

Earthquake	Evaluation criteria							
	J_1	J_2	J_3	J_4	J_5	J_6	J_7	J_8
Kobe	0.64	0.62	0.98	0.62	0.42	0.45	0.61	0.45
Northridge	0.64	0.64	0.92	0.65	0.39	0.40	0.51	0.40
El Centro	0.50	0.69	1.00	0.69	0.38	0.43	0.78	0.43
Hachinohe	0.61	0.58	1.00	0.57	0.39	0.41	0.51	0.41

interstory drift was observed; also, the normed criteria J_5 and J_6 were correspondingly smaller (39% and 40%, respectively). Satisfactory NES performance for the earthquakes of El Centro and Hachinohe was also found. In particular, 50% and 31% reductions for the El Centro earthquake and 39% and 42% reductions for the Hachinohe earthquake, respectively, for J_1 and J_2, were noted. Moreover, the performance of the VI NES holds in terms of normed criteria J_5 and J_6 as well (38% and 43% for El Centro and 39% and 41% for Hachinohe).

These results demonstrate that a VI NES optimized for one specific (but particularly severe) earthquake (Kobe) maintains its very good performance for the other three earthquakes having different frequency–energy characteristics, as highlighted in Section 2.

Hence, we can definitively state that the proposed VI NES Design I for the seismically excited shear frame structure is feasible and efficacious as an important element of an overall vibration control strategy. Moreover, this design appears to be robust, maintaining performance over four seismic excitations with different frequency and energy content. However, we note that, after the initial, high-energy stage of the response (during the strong ground motion), when the effectiveness of the VI NES is greatest, there follows a lower-energy stage where the amplitude of vibration is smaller and the performance of the VI NES deteriorates (in some cases it is possible to reach the no-impact condition, after which the VI NES is completely ineffective). Therefore, when the instantaneous seismic energy of the primary system with attached VI NES decreases sufficiently, the VI NES is no longer useful. Further, a VI NES designed to protect a structure against earthquakes of severe intensity may not be effective for earthquakes of moderate intensity. Therefore, in the next section we consider an alternative design for seismic mitigation, based on the use of combined NESs with smooth and non-smooth stiffness nonlinearities. This alternative design has the potential to provide effective seismic mitigation for both strong and moderate earthquake excitations.

4. Combination of VI and smooth NESs connected to different floors of the three-story frame (NES Design II)

In NES Design II, we consider a combination of a smooth NES connected to mass m_3 (the top floor) and a VI NES attached to mass m_1 (the first floor) of the primary system, as shown in Fig. 13. The intent behind this design is to combine a large-mass VI NES with a small-mass smooth NES in a design that is practically realizable [32]. By attaching a smooth NES to the top floor of the primary system, we can relax the requirement of relatively large mass ratios typical of the VI NES design and still obtain acceptable energy dissipation. In addition, the VI NES attached to the ground floor of the structure can assume a large mass ratio—and, hence, solid performance as shown previously—without any limitation from a practical point of view of design (since the VI NES can be directly supported by the foundation itself, and not by the structure). Moreover, a lightweight smooth NES is an effective absorber and dissipater of broadband shock energy from the primary structure to which it is attached; however, due to its relatively slower reaction time compared to the VI NES, we anticipate that the smooth NES will be more effective in the later, lower-energy regime of the seismic response, where the VI NES is less effective. Thus, the proposed NES Design II aims to provide effective seismic protection during both the initial, higher-energy regime of response (through the VI NES) and the later, lower-energy regime (through the smooth NES). This conjecture will be tested below.

The equations of motion governing the system can be expressed in the form

$$M\ddot{u}+C\dot{u}+Ku=-M\Gamma\ddot{u}_g+f, \tag{12}$$

where the mass, damping and stiffness matrices are given by

$$M=\begin{bmatrix} m_1 & 0 & 0 & 0 & 0\\ 0 & m_2 & 0 & 0 & 0\\ 0 & 0 & m_3 & 0 & 0\\ 0 & 0 & 0 & m_{NES1} & 0\\ 0 & 0 & 0 & 0 & m_{NES2}\end{bmatrix},\quad C=\begin{bmatrix} \lambda_1+\lambda_2 & -\lambda_2 & 0 & 0 & 0\\ -\lambda_2 & \lambda_2+\lambda_3 & -\lambda_3 & 0 & 0\\ 0 & -\lambda_3 & \lambda_3+\lambda_4 & 0 & -\lambda_4\\ 0 & 0 & 0 & 0 & 0\\ 0 & 0 & -\lambda_4 & 0 & \lambda_4\end{bmatrix},\quad K=\begin{bmatrix} 2k+k_{NES1} & -k & 0 & -k_{NES1} & 0\\ -k & 2k & -k & 0 & 0\\ 0 & -k & k & 0 & 0\\ -k_{NES1} & 0 & 0 & k_{NES1} & 0\\ 0 & 0 & 0 & 0 & 0\end{bmatrix} \tag{13}$$

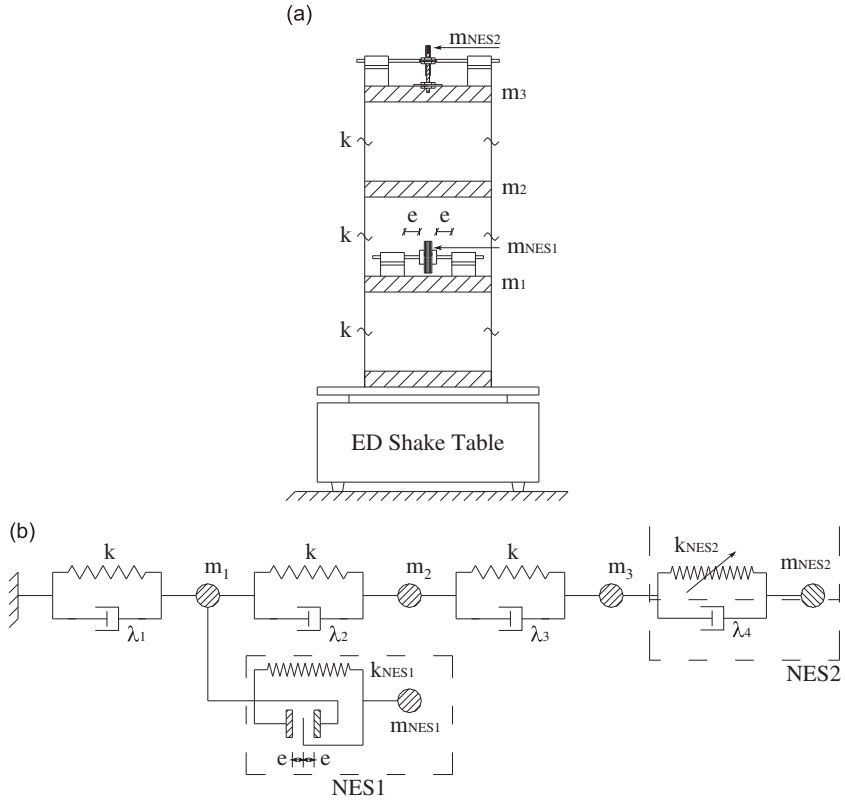

Fig. 13. NES Design II: three-story shear frame with smooth NES at the top floor and VI NES at the first floor: (a) schematic and (b) model.

and f represents the restoring force of the essentially nonlinear stiffness of the smooth NES (with nonlinearizable cubic nonlinearity),

$$f = \begin{bmatrix} 0 \\ 0 \\ -k_{NES2}(u_3-u_5)^3 \\ 0 \\ -k_{NES2}(u_5-u_3)^3 \end{bmatrix}. \tag{14}$$

Finally, $\ddot{u}_g$ represents the ground acceleration, and Γ the pseudo-static vector. Again the dynamic response of the system with attached VI and smooth NESs was simulated utilizing a Matlab code which computes precisely the time instants where vibro-impacts occur.

In this case, the optimization was performed with respect to both NESs, so in addition to the parameters relevant to the VI NES (i.e., weak linear coupling stiffness, clearance, mass, and coefficient of restitution) we included the following additional parameters for the smooth NES: the coefficient of the essentially nonlinear cubic stiffness, k_{NES2}; the mass, m_{NES2}; and the damping constant, λ_4 (cf. Fig. 13). The optimization was carried out for the scaled Kobe seismic excitation. As for NES Design I, the technique employed to optimize the parameters of the NESs in Design II is differential evolution [28,29]. As in the previous case, we aimed to control the structural response in terms of maximum displacements and maximum interstory drifts since these parameters are mainly related to structural damage. Therefore, our goal was to find the NES parameters that rendered minimum the sum of the evaluation criteria related to those kinematic parameters. In other words, our purpose was to minimize the objective function, $OF=J_1+J_2+J_5+J_6$, where J_1 and J_2 are non-normed criteria and J_5 and J_6 are normed criteria, related to the maximum displacement and maximum interstory drift, respectively.

The optimized parameters for the two sinks of NES Design II were found to be (i) for the VI NES (NES1 in Fig. 13), $m_{NES1}=2.4\%$ of the total mass of primary system, $e=0.011$ m, $r=0.426$, and $k_{NES1}=0.001\,k$; and (ii) for the smooth NES (NES2 in Fig. 13), $k_{NES2}/k=19\,\mathrm{m}^{-2}$, $\lambda_4/\lambda_3=3.277$, and $m_{NES2}=2.0\%$ of the total mass of primary system. We specified that the NES mass ratios, during the optimization, were allowed to vary from 0% to 2.5% in order to limit the total NES mass. For this particular set of optimized NES parameters, the comparison between the controlled and uncontrolled responses is depicted in Fig. 14; in the same figure we depict the displacement of the smooth NES. Fig. 15 depicts the displacement of the VI NES,

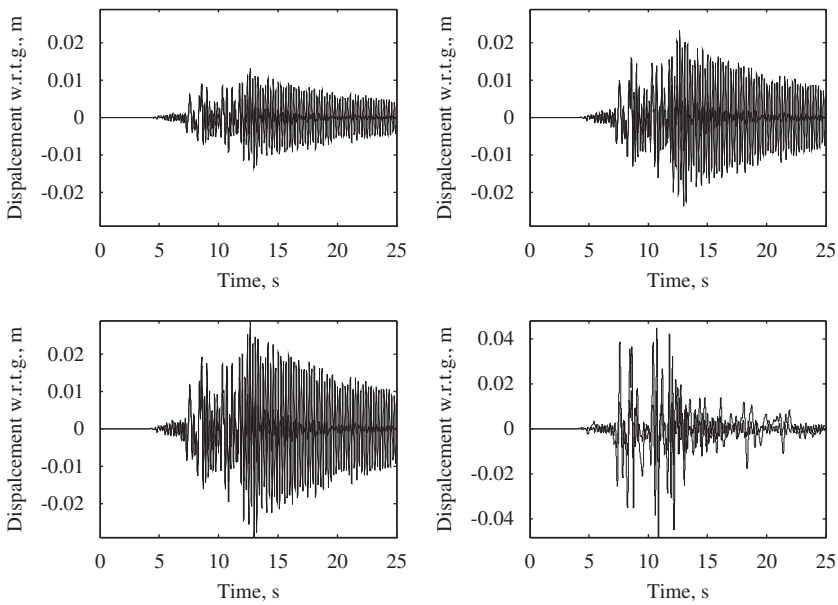

Fig. 14. Uncontrolled and controlled displacements for optimized NES Design II, for Kobe seismic excitation; u_j is the absolute displacement of the j-th floor. Dashed line, without NES; solid line, with NES.

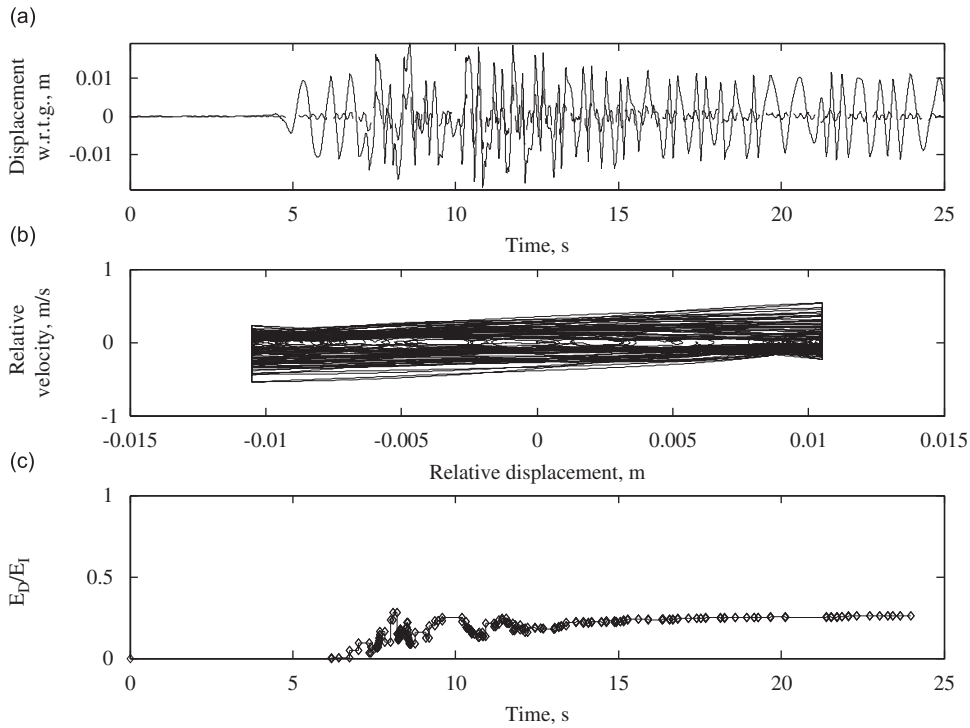

Fig. 15. NES Design II: performance of the optimized VI NES for Kobe seismic excitation: (a) comparison between absolute displacements of the first floor (darker line) and the VI NES (lighter line); (b) phase plot of relative displacement between the first floor and the VI NES; and (c) energy transaction by the VI NES (portion of instantaneous seismic energy dissipated during each vibro-impact).

the phase plot of the relative response between the first floor and the VI NES, and the time history of vibro-impacts (used to judge the severity of vibro-impacts in the optimized design).

To check the robustness of NES Design II, we examine the performance of the optimized two-NES configuration under seismic excitations corresponding to the remaining three test earthquakes. In Figs. 16 and 17 we depict the responses of the

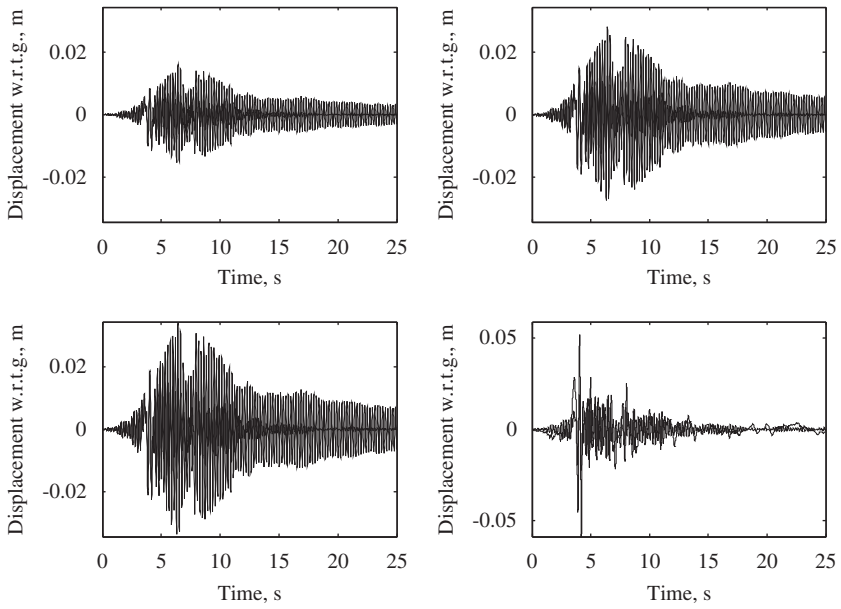

Fig. 16. Uncontrolled and controlled displacements for optimized NES Design II for Northridge seismic excitation (NESs parameters optimized for the earthquake of Kobe); u_j is the absolute displacement of the j-th floor. Dashed line, without NES; solid line, with NES.

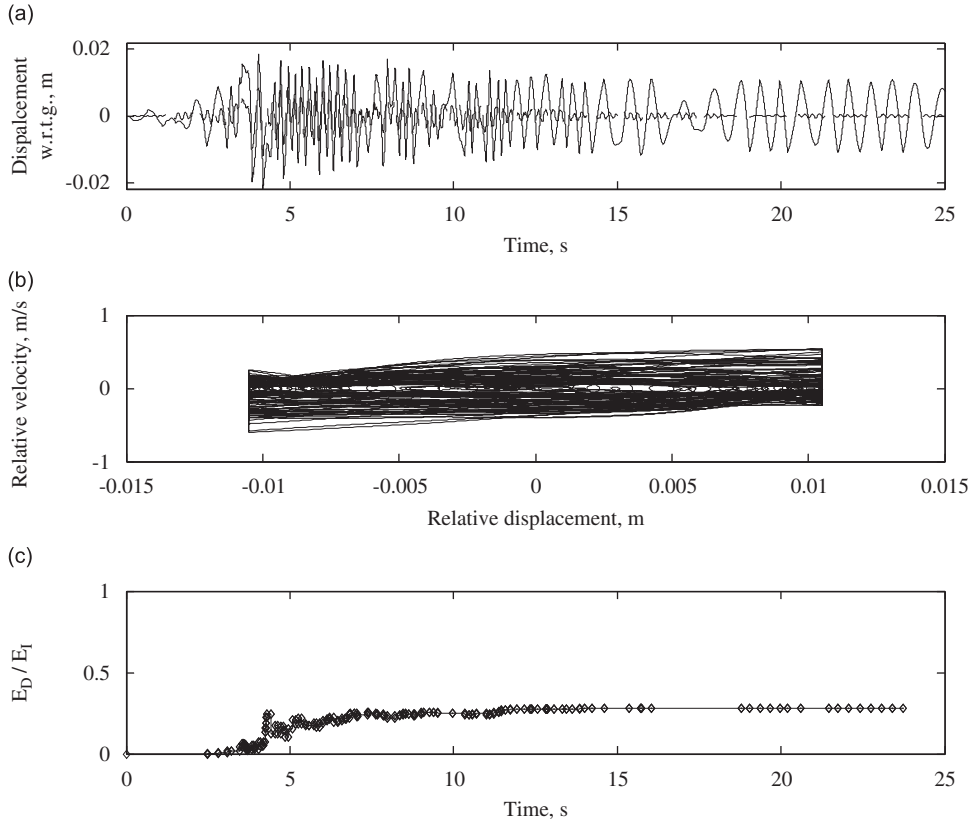

Fig. 17. NES Design II: performance of the optimized VI NES for Northridge seismic excitation: (a) comparison between absolute displacements of the first floor (darker line) and the VI NES (lighter line); (b) phase plot of relative displacement between the first floor and the VI NES; and (c) energy transaction by the VI NES (portion of instantaneous seismic energy dissipated during each vibro-impact).

system with NES Design II for time-scaled Northridge earthquake excitation, while using the NES parameters optimized for the Kobe earthquake. The quantitative evaluation criteria are summarized in Table 7. We note that the portion of seismic energy dissipated by the VI NES for Kobe and Northridge seismic excitations (see Figs. 15 and 17, respectively) is in the range of 25–30%. This percentage is smaller than in the previous NES Design I, where a single VI NES was connected to the top floor; this result is expected because in NES Design II the mass ratio of the VI NES is smaller and therefore the momentum exchange between the frame and the VI NES—and the consequent energy dissipation by the VI NES—is smaller as well.

From Table 7 we note that for Kobe earthquake excitation (for which NES Design II was optimized) we get better performance for NES Design II in terms of both non-normed (J_1, J_2, J_3, and J_4) and normed (J_5, J_6, J_7, and J_8) evaluation criteria. Considering the Northridge excitation (which, like the Kobe earthquake, possesses high energy content), we find results similar to those of NES Design I. We note an improvement in terms of criteria J_3 and J_7, while the reduction of maximum relative displacement decreases slightly from 36% to 30% (which can still be characterized as satisfactory performance). Considering the earthquakes of El Centro and Hachinohe (with much smaller energy content and, consequently, smaller possibility for TRC, which requires that the energy be above a threshold value), we note that there is an improvement of performance in terms of normed criteria for NES Design II compared to NES Design I. As pointed out previously, after moving the VI NES from the top floor to the first, the vibro-impacts result in smaller momentum exchanges and less energy dissipation. This is confirmed by Figs. 18 and 19, where the wavelet spectra show that the

Table 7
Summary of the evaluation criteria for different earthquakes, VI NES at the first floor and smooth NES at the top floor.

Earthquake	Evaluation criteria							
	J_1	J_2	J_3	J_4	J_5	J_6	J_7	J_8
Kobe	0.58	0.62	0.65	0.69	0.39	0.40	0.42	0.43
Northridge	0.63	0.70	0.76	0.66	0.39	0.41	0.42	0.41
El Centro	0.53	0.60	0.68	0.62	0.40	0.40	0.52	0.50
Hachinohe	0.80	0.87	0.86	0.87	0.38	0.39	0.45	0.42

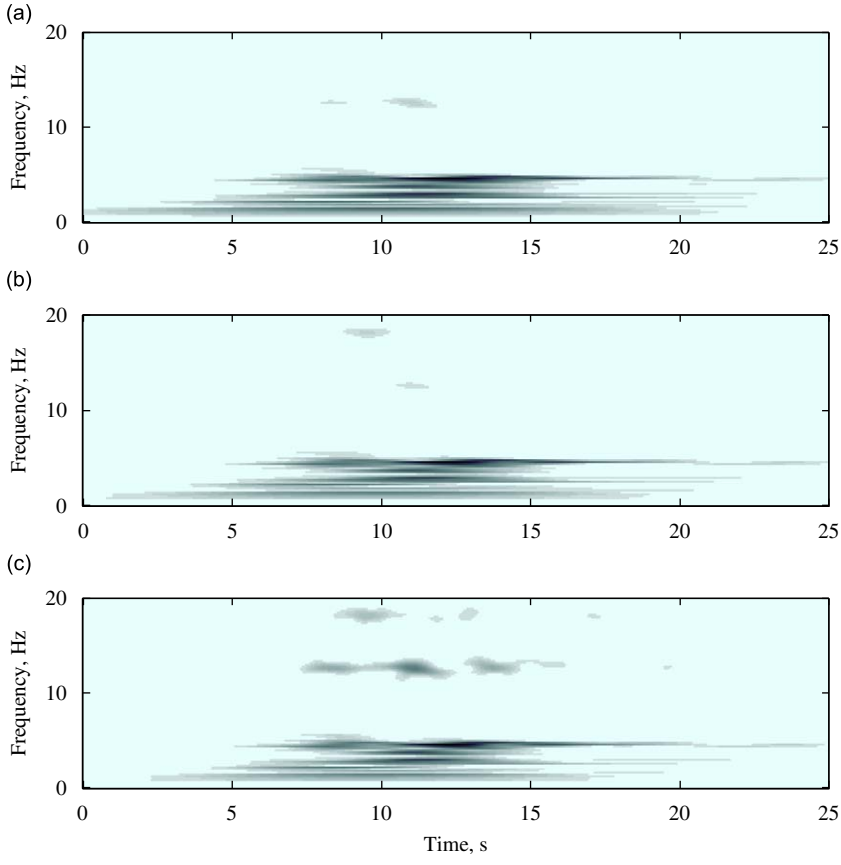

Fig. 18. Wavelet spectra of controlled relative displacements for a primary system with optimized VI NES attached to the first floor, smooth NES at the top floor (NES Design II), and Kobe seismic excitation: (a) $u_1(t)-u_g(t)$, (b) $u_2(t)-u_1(t)$, and (c) $u_3(t)-u_2(t)$.

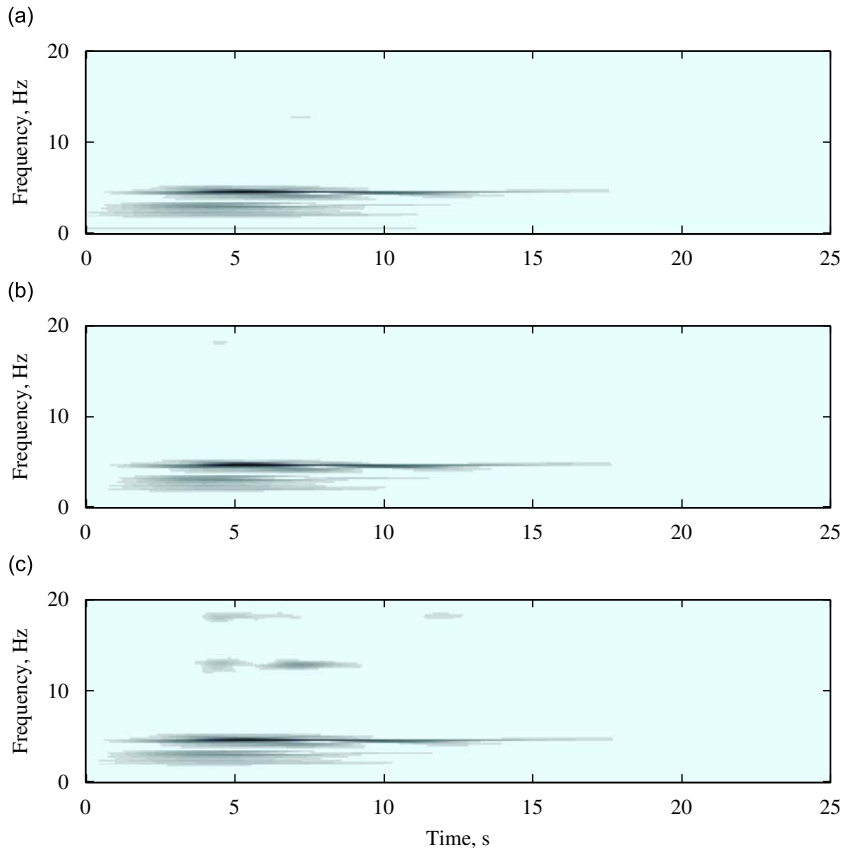

Fig. 19. Wavelet spectra of controlled relative displacements for a primary system with optimized VI NES attached to the first floor, smooth NES at the top floor (NES Design II), and Northridge seismic excitation: (a) $u_1(t)-u_g(t)$, (b) $u_2(t)-u_1(t)$, and (c) $u_3(t)-u_2(t)$.

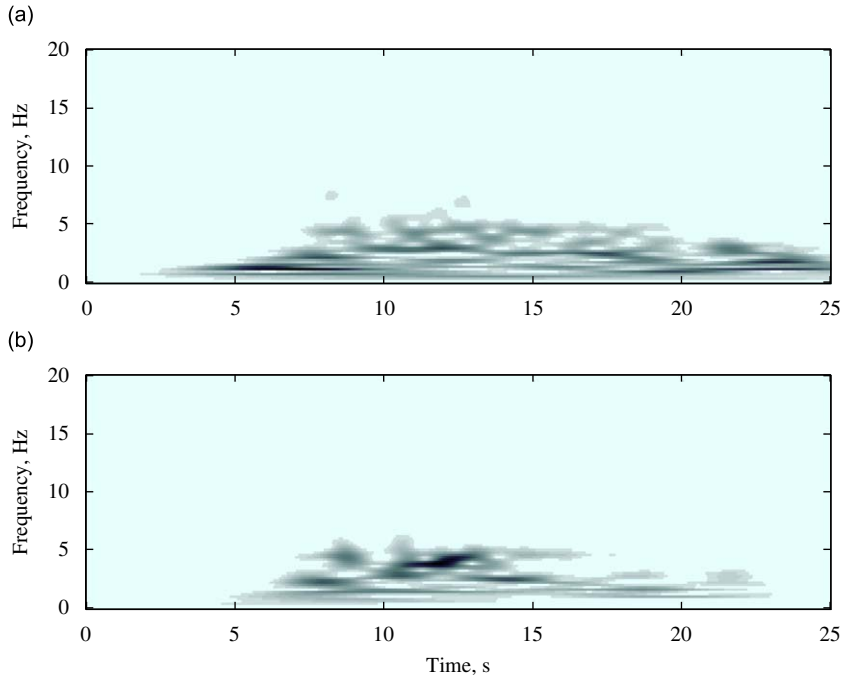

Fig. 20. Wavelet spectra of controlled relative displacements for a primary system with optimized VI NES attached to the first floor, smooth NES at the top floor (NES Design II), and Kobe seismic excitation: (a) $u_{\mathrm{VI-NES}}(t)-u_1(t)$ and (b) $u_{\mathrm{Smooth\ NES}}(t)-u_3(t)$.

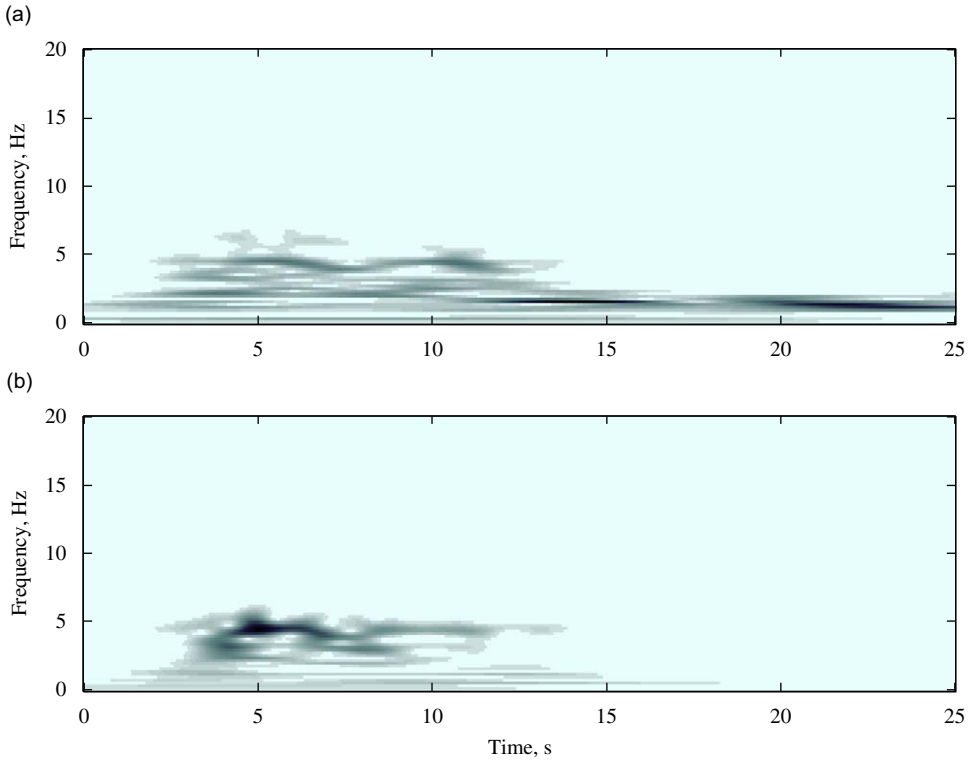

Fig. 21. Wavelet spectra of controlled relative displacements for a primary system with optimized VI NES attached to the first floor, smooth NES at the top floor (NES Design II), and Northridge seismic excitation: (a) $u_{\mathrm{VI-NES}}(t)-u_1(t)$ and (b) $u_{\mathrm{Smooth\ NES}}(t)-u_3(t)$.

energy scattering towards higher modes is less pronounced compared to that observed with NES Design I; we note that in Design I the mass of the VI NES was 4.0% of the total mass of the structure, which is almost twice the mass of the VI NES in Design II. Finally, we observe in Figs. 20 and 21 that in this case energy is pumped more vigorously out of the first mode (this phenomenon is more visible for the Northridge earthquake). The high amplitudes of the wavelet spectra in this case indicate that a TRC under conditions of strong ground motion takes place, accompanied by TET at the first linearized frequency of the structure; this TRC lasts for a few seconds, after which escape from resonance capture occurs.

5. Concluding remarks

We have applied the concepts of targeted energy transfer (TET) and the nonlinear energy sink (NES) to seismic mitigation of a three-story shear-frame structure subjected to four historic earthquakes, which were scaled to cause severe seismic excitation of the model structure. We showed numerically how it is possible to direct a significant portion of seismic energy from the primary structure toward the NES or set of NESs, where this energy is confined and locally dissipated. Thus, we have demonstrated that the nonlinear dynamic phenomenon of TET can be applied successfully to seismic mitigation.

In this work NESs with both smooth (cubic) and non-smooth (vibro-impact—VI) stiffness nonlinearities were considered. The novel aspect of applying a VI NES is twofold. First, it is possible to significantly and rapidly reduce the level of seismic structural response, especially in the initial stage of the response when the energy of the system is at its highest and the potential for structural damage is greatest. Second, vibro-impacts at the NES redistribute the seismic energy over wide frequency ranges, to lower and higher structural modes; as a result, the response of the primary structure is significantly reduced, because higher structural modes generally exhibit lower amplitudes of vibration and dissipate energy more efficiently.

Furthermore, we showed that a combination of NESs with smooth and nonsmooth nonlinearities, when optimized, can further reduce the seismic response of the primary structure. In general, a VI NES is most effective when attached to the ground floor of the primary structure; this is due to the requirement for relatively large mass of the VI NES for optimal performance. In contrast, an NES with smooth nonlinearity is more effective when attached to a higher floor of the structure, because its capacity to passively absorb and locally dissipate seismic energy is enhanced when its mass is light [29–32,34]. Moreover, at higher floors the levels of structural vibration are higher, which facilitates the activation of the essential stiffness nonlinearity of this type of NES.

Two different NES designs were considered in this work, embodying a single VI NES on the top floor (Design I), and a combination of a VI NES on the first floor and an NES with smooth stiffness nonlinearity on the top floor (Design II). By

performing optimization studies by means of genetic algorithms, we were able to demonstrate that both optimized NES designs lead to significant passive reduction of the seismic response of the three-story shear-frame structure. However, an optimized two-NES design (Design II) was capable of (i) reducing the NES mass at the top floor (with respect to Design I) and (ii) improving the overall structural response, as quantified through a set of objective criteria. Moreover, positive synergy of the two NESs appears to materialize in Design II, with the heavier VI NES at the bottom floor being more effective for strong (near-field) seismic excitation and the lighter NES with smooth stiffness nonlinearity being more effective for moderate (far-field) seismic excitation as well as during the later, lower-energy phase of the motion induced by near-field excitation. Therefore, Design II appears to be suitable for structural seismic mitigation against both strong, near-field earthquakes and far-field earthquakes of modest intensity.

Acknowledgment

This research was partially supported by the US National Science Foundation though Grant no. CMS—0324433.

References

[1] O. Gendelman, L.I. Manevitch, A.F. Vakakis, R. M'Closkey, Energy pumping in nonlinear mechanical oscillators: Part I—Dynamics of the underlying Hamiltonian systems, *Journal of Applied Mechanics* 68 (2001) 34–41.
[2] A.F. Vakakis, Shock isolation through the use of nonlinear energy sinks, *Journal of Vibration and Control* 9 (1–2) (2003) 79–93.
[3] G.W. Housner, L.A. Bergman, T.K. Caughey, A.G. Chassiakos, R.O. Claus, S.F. Masri, R.E. Skelton, T.T. Soong, B.F. Spencer, J.T.P. Yao, Structural control: past, present and future, *ASCE Journal of Engineering Mechanics* 123 (9) (1997).
[4] S.W. Shaw, R.H. Rand, The transition to chaos in a simple mechanical system, *International Journal of Nonlinear Mechanics* 24 (1989) 41–56.
[5] V.I. Babitsky, *Theory of Vibro-impact Systems*, Springer Verlag, Berlin and New York, 1998.
[6] B. Brogliato, *Nonsmooth Mechanics*, Springer Verlag, Berlin and New York, 1999.
[7] S.G. Kryzhevich, V.A. Pliss V.A., Chaotic modes of oscillation of a vibro-impact system, *Journal of Applied Mathematics and Mechanics—Prikladnaya Matematika I Mekhanika* 69 (2005) 13–26.
[8] P. Thota, H. Dankowicz, Continuous and discontinuous grazing bifurcations in impacting oscillators, *Physica D* 214 (2006) 187–197.
[9] S.F. Masri, T.K. Caughey, On the stability of the impact damper, *Journal of Applied Mechanics* 33 (3) (1966) 586–592.
[10] S.F. Masri, A.M. Ibrahim, Response of the impact damper to nonstationary random excitation, *Journal of the Acoustical Society of America* 53 (1) (1973) 200–211.
[11] B. Blazejczyk-Okolewska, Analysis of an impact damper of vibration, *Chaos, Solitons and Fractals* 12 (2001) 1983–1988.
[12] F. Peterka, B. Blazejczyk-Okolewska B., Some aspects of the dynamical behavior of the impact damper, *Journal of Vibration and Control* 11 (2005) 459–479.
[13] R.I. Leine, H. Nijmeijer, *Dynamics and Bifurcations in Non-Smooth Mechanical Systems*, Springer-Verlag, Berlin and New York, 2004.
[14] F. Pfeiffer, C. Glocker, Contacts in multibody systems, *Journal of Applied Mathematical Mechanics* 64 (5) (2000) 773–782.
[15] A.F. Filippov, *Differential Equations with Discontinuous Righthand Sides*, Kluwer Academic Publishers, Dordrecht, 1988.
[16] F. Georgiadis, A.F. Vakakis, D.M. McFarland, L.A. Bergman, Shock isolation through passive energy pumping caused by non-smooth nonlinearities, *International Journal of Bifurcation and Chaos* 15 (6) (2005) 1–13.
[17] F. Nucera, A.F. Vakakis, D.M. McFarland, L.A. Bergman, G. Kerschen, Targeted energy transfer in vibro-impact oscillators for seismic mitigation, *Nonlinear Dynamics* 50 (3) (2007) 651–677.
[18] F. Nucera, Nonlinear energy pumping as a strategy for seismic protection, PhD thesis, University of Calabria at Arcavacata of Rende—Cosenza, Italy, 2005.
[19] D. Quinn, R.H. Rand, The dynamics of resonance capture, *Nonlinear Dynamics* 8 (1995) 1–20.
[20] A.F. Vakakis, L.I. Manevitch, Yu.V. Mikhlin, V.N. Pilipchuk, A.A. Zevin, *Normal Modes and Localization in Nonlinear Systems*, Wiley Interscience, New York, 1996.
[21] A.I. Neishtadt, Scattering by resonances, *Celestial Mechanics and Dynamical Astronomy* 65 (1997) 1–20.
[22] B.F. Spencer Jr., R.E. Christenson, S.J. Dyke, Next generation benchmark control problem for seismically excited buildings, *Proceedings of the Second World Conference on Structural Control*, Vol. 2, Wiley, New York, 1999, pp. 1135–1360.
[23] V. Perrier, T. Philipovitch, C. Basdevant C., Wavelet spectra compared to Fourier spectra, *Journal of Mathematical Physics* 36 (1995) 1506–1519.
[24] T.P. Le, P. Argoul, Continuous wavelet transform for modal identification using free decay response, *Journal of Sound and Vibration* 277 (2004) 73–100.
[25] J.P. Conte, H. Pandit, J.P. Stewart, J. Wallace, Ground motion intensity measures for performance-based earthquake engineering, In: Proceedings of the Ninth International Conference on Applications of Statistics and Probability in Civil Engineering (ICASP9), San Francisco CA, 2003, pp. 1465–1472.
[26] M.D. Trifunac, A.G. Brady, A study of the duration of strong earthquake ground motion, *Bulletin of the Seismological Society of America* 65 (1975) 581–626.
[27] E. Emaci, T.A. Nayfeh, A.F. Vakakis, Numerical and experimental study of nonlinear localization in a flexible structure with vibro-impacts, *Zeitschrift fur Angewandte Mathematik und Mechanik (ZAMM)* 77 (7) (1997) 527–541.
[28] R. Storn, K. Price, Differential evolution—a simple and efficient adaptive scheme for global optimization over continuous spaces, *Journal of Global Optimization* 11 (1997) 341–359.
[29] G. Kerschen, On the model validation in non-linear structural dynamics, PhD thesis, University of Liege, Department of Aerospace, Mechanics and Materials Engineering, 2002.
[30] G. Kerschen, A.F. Vakakis, Y.S. Lee, D.M. McFarland, J. Kowtko, L.A. Bergman, Energy transfers in a system of two coupled oscillators with essential nonlinearity: 1:1 resonance manifold and transient bridging orbits, *Nonlinear Dynamics* 42 (3) (2005) 283–303.
[31] G. Kerschen G., Y.S. Lee, A.F. Vakakis, D.M. McFarland, L.A. Bergman, Irreversible passive energy transfer in coupled oscillators with essential nonlinearity, *SIAM Journal on Applied Mathematics* 66 (2) (2006) 648–679.
[32] O. Gendelman, G. Kerschen, A.F. Vakakis, L. Bergman, D.M. McFarland, Impulsive periodic and quasiperiodic orbits in a system of coupled oscillators with essential stiffness nonlinearity, *Communications in Nonlinear Science and Numerical Simulation* 13 (5) (2008) 957–978.
[33] A.F. Vakakis, O. Gendelman, Energy pumping in nonlinear mechanical oscillators: Part II—resonance capture, *Journal of Applied Mechanics* 68 (2001) 42–48.
[34] V.I. Arnold (Ed.), *Dynamical Systems III, Encyclopaedia of Mathematical Sciences*, Vol. 3, Springer Verlag, Berlin and New York, 1988.
[35] Y.S. Lee, G. Kerschen, A.F. Vakakis, P.N. Panagopoulos, L.A. Bergman, D.M. McFarland, Complicated dynamics of a linear oscillator with a light, essentially nonlinear attachment, *Physica D* 204 (1-2) (2005) 41–69.